The large-scale structure around the Fornax-Eridanus Complex

M. A. Raj[1], P. Awad[1,2], R. F. Peletier[1], R. Smith[3], U. Kuchner[4], R. van de Weygaert[1], N. I. Libeskind[5], M. Canducci[6], P. Tiňo[6], and K. Bunte[2]

[1] Kapteyn Astronomical Institute, University of Groningen, PO Box 800, 9700 AV Groningen, The Netherlands
 e-mail: `m.a.raj@rug.nl`
[2] Bernoulli Institute for Mathematics, Computer Science and Artificial Intelligence, University of Groningen, 9700AK Groningen, The Netherlands
[3] Departamento de Física, Universidad Técnica Federico Santa María, Avenida Vicuña Mackenna 3939, San Joaquín, Santiago de Chile
[4] School of Physics, Astronomy, University of Nottingham, Nottingham NG7 2RD, United Kingdom
[5] Leibniz-Institute für Astrophysik Potsdam (AIP), An der Sternwarte 16, D-14482 Potsdam, Germany
[6] School of Computer Science, University of Birmingham, Birmingham B15 1TT, United Kingdom

Received xxx; accepted yyy

ABSTRACT

Aims. Our objectives are to map the filamentary network around the Fornax-Eridanus Complex and probe the influence of the local environment on galaxy morphology.

Methods. We employ the novel machine-learning tool, 1-DREAM (1-Dimensional, Recovery, Extraction, and Analysis of Manifolds) to detect and model filaments around the Fornax cluster. We then use the morphology-density relation of galaxies to examine the variation in the galaxies' morphology with respect to their distance from the central axis of the detected filaments.

Results. We detect 27 filaments that vary in length and galaxy-number density around the Fornax-Eridanus Complex. We find that 81% of galaxies in our catalogue belong to filaments and 19% of galaxies are located outside filaments. The filaments around the Fornax-Eridanus Complex showcase a variety of environments; some filaments encompass groups/clusters, while others are only inhabited by galaxies in pristine filamentary environments. In this context, we reveal a well-known structure – the *Fornax Wall*, that passes through the Dorado group, Fornax cluster, and Eridanus supergroup. With regard to the morphology of galaxies, we find that early-type galaxies (ETGs) populate high-density filaments and high-density regions of the Fornax Wall. Furthermore, the fraction of the ETG-population decreases as the distance to the central axis of the filament increases. The fraction of late-type galaxies (LTGs; 8%) is lower than that of ETGs (12%) at 0.5 Mpc/h from the filament spine. Of the total galaxy population in filaments around the Fornax-Eridanus Complex, ∼ 7% are ETGs and ∼ 24% are LTGs located in pristine environments of filaments, while ∼ 27% are ETGs and ∼ 42% are LTGs in groups/clusters within filaments. Among the galaxies in the filamentary network around the Fornax-Eridanus Complex, 44% of them belong to the Fornax Wall.

Conclusions. This study reveals the Cosmic Web around the Fornax Cluster, which exhibits a variety of filamentary environments. With this, our research asserts that filamentary environments are heterogeneous in nature. When investigating the role of the environment on galaxy morphology, it is essential to consider both, the local number-density and a galaxy's proximity to the filament spine (*filament core*). Within this framework, we ascribe the observed morphological segregation in the Fornax Wall to pre-processing of galaxies within groups embedded in it.

Key words. Cosmology: large-scale structure of Universe – Galaxies: evolution – Galaxies: clusters: individual: Fornax – Galaxies: groups: individual: Eridanus – Galaxies: groups: individual: Dorado

1. Introduction

The large-scale distribution of matter and galaxies forms a web-like structure called the *Cosmic Web* (Bond et al. 1996). Early attempts to map the Universe (Jõeveer et al. 1978; Geller & Huchra 1989; Bond et al. 1996; van de Weygaert & Bond 2008; van de Weygaert & Schaap 2009; Tempel et al. 2014; Courtois et al. 2013; Cautun et al. 2014a) revealed an intricate pattern containing structures extending from a few megaparsecs to several hundreds of megaparsecs. In a ΛCDM paradigm, these structures form hierarchically under the influence of gravity (White & Rees 1978), and the *Cosmic Web* is therefore an accumulation of *galaxies, gas*, and *dark matter* in dense clusters, connected by filaments and walls, and separated by voids. Several galaxy redshift surveys (e.g. Colless et al. 2001; Skrutskie et al. 2006; Tegmark et al. 2004; Huchra et al. 2012; DESI Collaboration

et al. 2023) have confirmed the web-like network of galaxies. Likewise, N-Body simulations (e.g. Vogelsberger et al. 2014; Springel 2005; Schaye et al. 2015) of the Cosmic Web and cosmic density field reconstruction (e.g. Kitaura 2013) have also displayed the spatial pattern of galaxies as well as dark matter (e.g. Heß et al. 2013; Sorce et al. 2016; Kitaura et al. 2024; Malavasi et al. 2023).

The densest parts of the Cosmic Web are groups and clusters (sometimes called nodes) which may be part of superclusters (de Vaucouleurs 1958; Einasto et al. 2003, 2011a; Liivamägi et al. 2012) of galaxies, and these superclusters may be embedded in walls (Einasto et al. 2010, 2017). In this context, Einasto et al. (2024) showed that very rich clusters are located in superclusters and luminous groups and clusters are within or near filaments. Supercluster-Complexes are structures of several nearly connected, very rich superclusters, such as the Sloan Great Wall

(Gott et al. 2005) and the BOSS Great Wall (Lietzen et al. 2016). Additionally, superclusters can form vast planes spanning hundreds of megaparsecs, like the Local Supercluster Plane or the Dominant Supercluster Plane (Einasto et al. 1983, 1997; Peebles 2023). Studies pertaining to superclusters (e.g. Araya-Melo et al. 2009; Chon et al. 2014; Tully et al. 2014; Kraan-Korteweg et al. 2017; Haines et al. 2018; Einasto et al. 2021; Bag et al. 2023; Hatamkhani et al. 2023, and references therein) showed that they are distinct in terms of their dynamical state, galaxy populations, and size. For example, Venturi et al. (2022) detected minor mergers of galaxy-groups within the Shapely (Shapley 1930) supercluster, the largest known gravitationally bound system.

Galaxies flow from low-density regions to high-density regions and therefore experience various environments throughout their lifetime. As such, these environments vary in density, dynamical state, and composition. The impact of the local density on the morphology of galaxies has been well-established by the morphology-density relation by Dressler (1980), but understanding the additional effect of the topology or geometry of the physical environment of the Cosmic Web components is currently a topic of active research. Specifically, mechanisms acting in cluster and group environments have been shown to affect the star-formation of their member galaxies (e.g. Gunn & Gott 1972; Kauffmann et al. 2004; Boselli & Gavazzi 2006; Bamford et al. 2009; Vulcani et al. 2015; Brown et al. 2023). There is substantial observational evidence of the morphology-density relation in clusters and groups (Mei et al. 2023; Marasco et al. 2023, and references therein), wherein early-type galaxies (ETGs) are commonly found in high-density regions and late-type galaxies (LTGs) are prevalent in low-density regions. Einasto & Einasto (1987) were the first to show that the morphology-density relation extends from rich clusters to poor groups as well as isolated galaxies. Einasto (1992) also concluded that ETGs either belong to clusters or that they reside in small groups within filaments. However, the consequence of these occurrences is still a debate. In particular, it is still unclear whether density is a predominant cause for the formation of ETGs or that these galaxies formed at an earlier epoch. With regard to the low-stellar mass regime ($M_* = 10^7 - 10^9 M_\odot$), research (e.g. Román & Trujillo 2017; Benavides et al. 2023; For et al. 2023, to name a few) in the past decade has revealed evidence of the role of the environment on dwarf galaxies, with particular focus on their formation channels. The question persists as to the extent of environmental influence on the formation and evolution of dwarf galaxies. In fact, we are yet to investigate them in cosmic environments. However, the role of cosmic environments on the evolution of galaxies ($M_* \geq 10^9 M_\odot$) has been corroborated extensively, with some indication of overlapping densities in filaments, walls, and clusters (see Cautun et al. 2014a; Libeskind et al. 2018). In this context, the extent of this relation to large-scale structures (e.g. Kraljic et al. 2018; Einasto et al. 2022; Galárraga-Espinosa et al. 2023) is also an ongoing research topic. As such, there is evidence of a strong correlation of galaxies' properties such as colour, stellar mass, and star-formation, with regard to the distance to their filament spine (e.g. Chen et al. 2017; Kraljic et al. 2018; Castignani et al. 2022; Bulichi et al. 2023). Several theoretical explanations exist to explain this observed trend. For example, Aragon Calvo et al. (2019) proposed that star-formation of galaxies is quenched when they are detached from their primordial filaments.

Dark matter and baryonic matter are fed into clusters and groups through cosmic filaments (e.g. Aragón-Calvo et al. 2007; Cautun et al. 2013a; Galárraga-Espinosa et al. 2023; Cornwell et al. 2024), and within these filaments, galaxies start to experience "pre-processing" (Zabludoff & Mulchaey 1998; Balogh

et al. 2000; Fujita 2004). This term has a broad range of definitions in the literature, but overall, it includes all processes affecting the properties of galaxies before cluster-infall. There have been extraordinary evidences of pre-processing of galaxies, not just in groups accreting onto clusters (e.g. Kleiner et al. 2021; Bidaran et al. 2022; Lopes et al. 2024) but also in filaments (e.g Cybulski et al. 2014; Sarron et al. 2019; Chung et al. 2021). Kuchner et al. (2022) also demonstrated the heterogeneity of filament environments and the various pathways galaxies take before cluster-infall.

To investigate mass-accretion in the Cosmic Web and the impact of the large-scale environment on galaxy evolution, we require robust tools to classify large-scale structures. Libeskind et al. (2018) discussed the functionality of several such techniques. Some prominent examples are DisPerSE (Sousbie 2011), Bisous model (Tempel et al. 2014), Multi-scale morphology filter/NEXUS (Aragón-Calvo et al. 2007; Cautun et al. 2013b), V-web: velocity shear tensor (Libeskind et al. 2014), or T-REx (Tree-based Ridge Extractor; Bonnaire et al. 2020; Aghanim et al. 2024). Based on the objectives for classification and the methodologies in comparing the extracted components of the Cosmic Web, Libeskind et al. (2018) found that these different techniques yielded diverse results on the properties of the Cosmic Web despite several similarities. Another caveat is that the filamentary structures defined theoretically and observationally are those traced by massive galaxies, and this is due to the detection limit of current galaxy surveys (e.g. Cautun et al. 2014a). Hence, Cosmic Web classification methods should be reliable in detecting tenuous structures and optimised to include dwarf galaxies.

Our analysis is based on the novel toolbox for analysing the Cosmic Web, called 1-DREAM[1], an acronym for *1-Dimensional Recovery, Extraction, and Analysis of Manifolds.* 1-DREAM was first introduced by Canducci et al. (2022) and followed by this, Awad et al. (2023) demonstrated its application and reliability on N-body simulations. In brief, 1-DREAM comprises five different Machine Learning (ML) algorithms that serve the extraction and analysis of multi-dimensional structures within astronomical datasets. The functions performed by the algorithms range from detecting cosmic structures across varying densities and distinguishing the different environments of the Cosmic Web, to finding the central spines of the detected filaments and probabilistic modelling of the distribution of matter surrounding them. In addition to giving a detailed description of the functionality of 1-DREAM, Awad et al. (2023) applied it on the same cosmological N-body simulation used by Libeskind et al. (2018) as a common data set to compare it to many Cosmic Web-tracing methodologies. The toolbox produced comparable results to the state-of-the-art methods when separating the simulated particles between each Cosmic Web environment. Notably, Awad et al. (2023) showed that reducing the number of particles comprising filaments in cosmological simulations produced minimal change in the central axes retrieved for the same filaments. Such stability is not found in widely used Cosmic Web-tracing algorithms such as DisPerSE, where the down-sampling of data tends to cause visible changes in the retrieved axes. This advantage is crucial, considering the sparsity of galaxies per unit volume within observations in comparison to cosmological simulations of the Cosmic Web. Awad et al. (2023) also confirmed that the filament spines found by 1-DREAM tend to trace accurate paths that become highly stable references which in turn

---

[1] 1-DREAM is publicly available at `https://git.lwp.rug.nl/cs.projects/1DREAM`

allows accurate measurements of the properties of galaxies as a function of their distances to the axes. Finally, Awad et al. (2023) showed that 1-DREAM produces less false positive or negative detection of filaments when compared to DisPerSE. These advantages have motivated the use of 1-DREAM in our investigation of the large-scale structure of the Fornax-Eridanus Supercluster. The research presented here is both a first used-case for the 1-DREAM toolbox on observational data *and* the largest systematic analysis of galaxy pre-processing in the extended region of the Fornax-Eridanus Complex.

The Fornax-Eridanus Complex is at distance of 20 Mpc[2]. We aim to probe the Cosmic Web around this region and examine the role of the filamentary environment on the morphology of galaxies. The research presented in this article is also motivated by the wealth of imaging data currently available (and with upcoming data from the Euclid Survey; Euclid Collaboration et al. 2022) for the region around the Fornax cluster. This will allow us to investigate the influence of the large-scale environment on several observational properties of galaxies. Below, we give a literature review of the Fornax-Eridanus Complex.

The Southern Supercluster is a long strand of galaxies from Cetus to the Dorado group, passing through Fornax, Eridanus, and Horologium (de Vaucouleurs 1953, 1956). Fairall et al. (1994) described this supercluster as a "pancake structure" (flattened) that resembled a *Great Wall* and called it the Fornax Wall. Within this ensemble of galaxies, Nasonova et al. (2011) and Makarov & Karachentsev (2011) found that several groups were merging in the Fornax and Eridanus regions (see also Brough et al. 2006) albeit a majority of them are yet to reach dynamical equilibrium. The major systems forming the Fornax-Eridanus Complex are the Fornax cluster (NGC 1399) and its infalling subgroup (NGC 1316), the Eridanus supergroup (NGC 1302, NGC 1332, NGC 1395, NGC 1398, NGC 1407; see Brough et al. 2006), and the Dorado group (NGC 1553, NGC 1672). Nasonova et al. (2011) found that smaller systems such as galaxy pairs and triplets were merging with the Fornax cluster. Similarly, the groups within the Eridanus cloud will eventually merge to form a cluster with NGC 1407 as the Brightest Cluster Galaxy. The Cetus-Aries cloud (see de Vaucouleurs 1975; Tully 1987) comprises several groups, some of which belong to the Cetus I cloud (NGC 1052, NGC 1068) and the Cetus II cloud (NGC 0584, NGC 0681). On larger scales, the Southern supercluster is part of the Southern Supercluster Strand, which is a filament connecting to the Centaurus cluster (Courtois et al. 2013; Tully et al. 2014). The other branch of this Strand is the Telescopium-Grus Cloud, a low-density filament, which connects to the Southern Supercluster through the Cetus-Aries Cloud (Tully & Fisher 1987). Collectively, the two branches of the Southern Supercluster Strand are called SSCa (Fornax-Eridanus-Dorado) and SSCb (see Courtois et al. 2013); the Southern Supercluster Strand is in turn part of the Laniakea Supercluster (Tully et al. 2014).

The layout of this paper is as follows: We explain the dataset and method we employ in Sects. 2 and 3 respectively. In Sect. 4, we present our results of the detected filaments, followed by their analysis in Sect. 5. We then discuss the role of the large-scale environment on galaxy morphology in Sect. 6. Finally, we summarise our results, draw conclusions of the same, and portray

our future perspectives of this study in Sect. 7. We provide supplementary information in Appendix A.

2. Data

Our analysis is based on the galaxy-group catalogue by Tempel et al. (2016) (hereafter T16a) which was constructed using data from the Extragalactic Distance Database (EDD, Tully et al. 2009). The dataset used by T16a is primarily based on the 2MASS Redshift Survey data (Huchra et al. 2012). To complement this, T16a also included redshift sources from the 2M++[3] survey (Lavaux & Hudson 2011), as well as CosmicFlows-2 (Tully et al. 2013). In brief, T16a employed the friends-of-friends algorithm in cosmology (see Tempel et al. 2014 for procedure), which was introduced by Zeldovich et al. (1982) and Huchra & Geller (1982). Then, they used a Multivariate Gaussian Mixture Modelling approach to identify substructures within galaxy-groups. Finally, T16a removed galaxies which were not bound to groups based on a group's virial radius and escape velocity. Additionally, the redshift space distortions for groups were suppressed as part of their method (see also Tempel et al. 2014 for a detailed description about the Finger of God correction)[4]. The catalogue by T16a comprises 78378 galaxies of which, 43480 are brighter than $K_S < 11.75$ mag (from the 2MASS Redshift Survey), 3627 do not have measured K_s magnitudes (CosmicFlows-2), and the remaining from 2M++ go down to $K_s < 12.5$ mag. This catalogue is complete for galaxies with $K_s < 11.5$ mag, which corresponds to $\log_{10}(M_*/M_\odot) = 8.40$ at a distance of 10 Mpc (Dálya et al. 2018; Ducoin et al. 2020). Therefore, this catalogue includes the brightest dwarf galaxies as well as more massive galaxies. Comparing to the Local Group, this would include galaxies such as the Large Magellanic Cloud, M33, M31, and our Milky Way. As the research presented in this article focuses on the region surrounding the Fornax-Eridanus supercluster, we extracted a subset of $r = 20$ Mpc/h, which we show in Fig. 1; the total number of galaxies within this subset is 933. Hereafter, we refer to this subset unless the original dataset is mentioned explicitly.

3. Method

We employ 1-DREAM to extract filamentary structures around the Fornax-Eridanus Complex. In this section, we summarise 1-DREAM, its usage, and the procedure we adopted to extract filaments from real data.
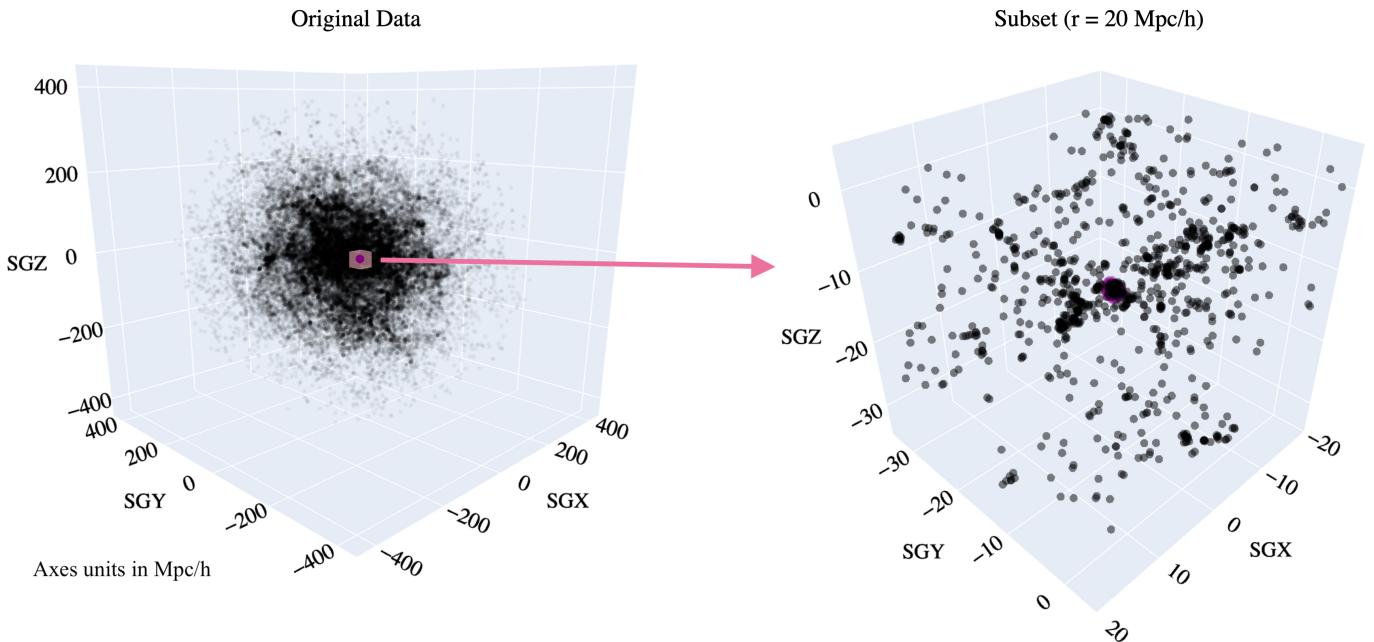
3.1. 1-DREAM

Here, we list the five algorithms within the toolbox, the acronyms used to refer to each of them, and their corresponding functions (for a detailed mathematical description, see Canducci et al. 2022 and Awad et al. 2023):

1. Locally Aligned Ant Technique (LAAT): It initiates a random walk through the data and distributes an artificially defined quantity termed the "pheromone" in reliance on the concept of Ant Colony dynamics. The random walk is guided

---

[2] The Fornax cluster (GLON = 236.7163°; GLAT = −53.6356°) is located in the southern Galactic hemisphere (for reference, our Milky Way is at GLON = 359.9443° and GLAT= −0.0461°) and the Virgo cluster (GLON = 283.7775°; GLAT = 74.4912°) is in the north Galactic hemisphere (see Fig. 12 and Sect. 10 of Kourkchi & Tully 2017).

[3] The 2M++ survey is based on data from the Two-Micron-All-Sky (Skrutskie et al. 2006) Source Catalogue and the 6dF Galaxy Survey (Jones et al. 2009).

[4] This correction is an essential step to perform, otherwise the Fingers of God will appear as over-densities in the data, and so will be mistaken by our methodologies as real filaments.

Original Data   Subset (r = 20 Mpc/h)

Fig. 1. Three-dimensional distribution of galaxies from the group catalogue by Tempel et al. (2016) represented in supergalactic coordinates (SGX, SGY, SGZ). The selected data with $r = 20$ Mpc/h centred on the Fornax cluster is highlighted in a pink mesh on the *left* panel and the zoomed-in cube is displayed on the *right* panel.
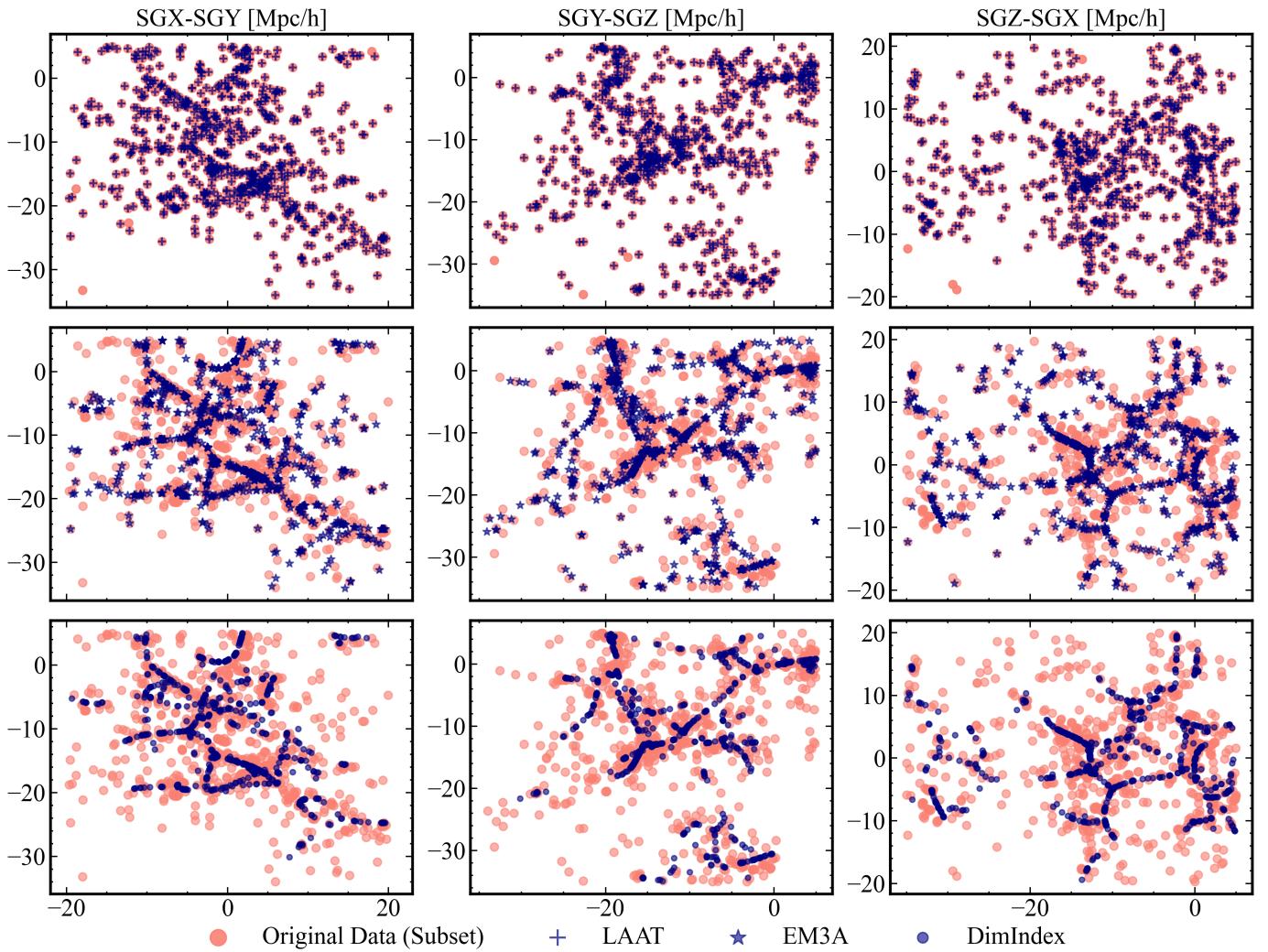
through the stipulation that local jumps between the points are more likely to occur if these points are aligned along a low-dimensional spatial structure. Running LAAT allows the pheromone to be concentrated in regions of high density and regions aligned with locally detected manifolds or structures. The pheromone quantity therefore acts as a positive feedback mechanism which enhances the contrast between low-density and high-density regions, and can be used as a threshold parameter to separate regions of varying density (Taghribi et al. 2023).

2. Evolutionary Manifold Aligned Aware Agents (EM3A): This collapses the positions of data points belonging to a structure onto that structure's central axis. The resulting distribution of points traces the spines of the structures detected in the previous step (Mohammadi & Bunte 2020). We refer to this spine as the filament core.

3. Dimensionality Index (DimIndex): It distinguishes the underlying dimensionality of the local structures that the particles/points belong to, which in turn allows the separation of 1-dimensional, 2-dimensional, and 3-dimensional (3D) structures (Canducci et al. 2022).

4. Multi-manifold Crawling (MMCrawling): It partitions the data into a set of filaments represented by their central axis and the group of particles surrounding them. Through this step, the spines (*filament core*) are also represented by graphs, that is, a series of nodes connected together by edges (Canducci et al. 2022).

5. Stream Generative Topographic Mapping (SGTM): This models the points belonging to each structure using a constrained Gaussian Mixture Model aligned along that structure. The purpose of this probabilistic modelling is to relax the idea that a structure begins and ends at a definite position. The model replaces this concept with a likelihood to belong to a structure instead (Canducci et al. 2022).

In this particular application, the data points on which the algorithms run are the individual galaxies in our sample. With regard to our current data selection, these different algorithms can be used consecutively in the following way: LAAT is used to highlight galaxies that belong to local structures present in the subset and allows their extraction from the data. EM3A can then be used to find the central axis running through the detected structures. DimIndex then separates the galaxies between those belonging to large clusters, walls, filaments, and voids. In this way, we isolate all detected filaments within the subset. MM-Crawling is then used to create a catalogue of all central axes of the filaments as well as the galaxies surrounding them, up to a given distance. In the creation of this catalogue, MMCrawling represents the axes as graph objects as explained above. The subsequent step would be to use SGTM to regularise the position of the embedded graph nodes and model the distribution of galaxies. Due to the probabilistic nature of SGTM, a densely-sampled manifold is essential to train and obtain Maximum Likelihood Estimates of its parameters. However, the sparsity of the subset at hand is not adequate to sample the filaments. Thus, in order to avoid over-fitting the model parameters of the available data, we did not use SGTM as part of the analysis in this research. When working with simulations that tend to be more populated, we recommend the usage of SGTM as a final step of applying 1-DREAM.

3.2. 1-DREAM usage and optimised-Crawling on real data

All algorithms within 1-DREAM rely on the idea of local neighbourhoods and localised Principal Component Analysis (PCA). In this context, local neighbourhoods are defined as spherical regions of a given radius r centred on each galaxy. Through PCA, we infer the local eigen-directions in which the galaxies are distributed within their neighbourhood (defined by the aforementioned radius r). Within the toolbox, performing PCA in local
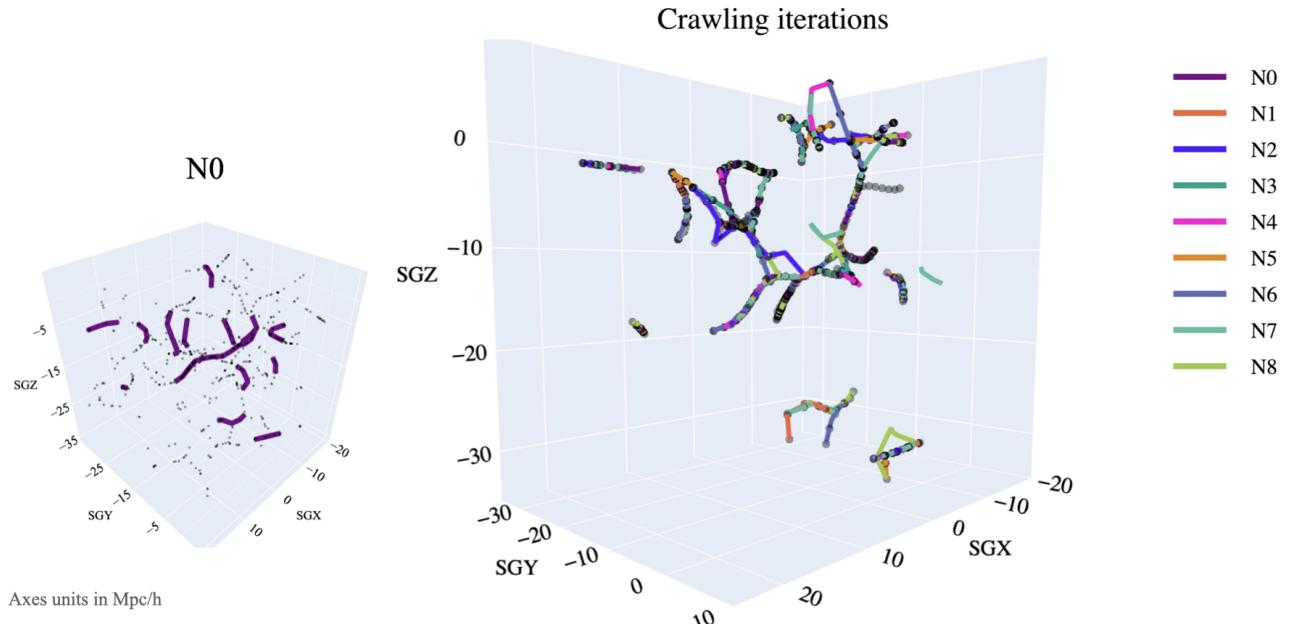
Fig. 2. Results of LAAT, EM3A, and DimIndex algorithms applied to our data. The first row depicts the structures highlighted by LAAT compared to the original distribution of galaxies. The second row shows the axes enhanced by EM3A. The third row shows the remaining 1-dimensional structures found by DimIndex. The results of each algorithm are drawn in blue and compared to the original distribution of data drawn in orange. The columns from left to right represent projections along the $x - y$, $y - z$, and $z - x$ planes.

neighbourhoods is the central step towards the intended function of each of its algorithms, and the size of the neighbourhoods plays a role in steering the PCA estimates. Adopting a very small radius acts as a zoomed-in perspective on the structures and might not include enough galaxies to infer correct information about their morphology. It would also lead to filtering out more than necessary galaxies as they get wrongly labelled as noise and not part of local structures. Similarly, choosing a neighbourhood radius that is larger than necessary leads to the inclusion of galaxies from multiple structures within the same neighbourhood and as a consequence, will bias the eigen-direction estimation and the conclusions regarding the morphology of the structures.

The neighbourhood radius parameter is normally chosen to be a small multiple of the expected structure-thickness in the data. Given that filament and wall diameters range from 1–7 Mpc/h (Cautun et al. 2014a), a suitable neighbourhood radius should lie within this range. Additionally, given the sparsity of the data, we expect to use a larger radius than what would be used for simulations to capture as much directional information

as possible. Through experimentation, we found that a neighbourhood radius of 3 Mpc/h produces the highest density contrast between the local structures and under-dense regions. It is also the least possible radius to use without visible structures getting eliminated by LAAT; this condition is crucial for recovering hidden structures within the region of interest. Therefore, we consistently adopted this radius throughout the application of 1-DREAM to our data. In order to preserve the structures which extend beyond our region of interest, we ran LAAT and EM3A on the entire (original) T16a dataset and from there, extracted the same subset, a data cube of side length of 40 Mpc/h, centred on the Fornax cluster. The particles which survived the threshold of LAAT are shown in the first row of Fig. 2. With EM3A, we recovered the central axes of the detected structures using the same value of the neighbourhood radius (3 Mpc/h). The resulting central axes are shown in the second row of Fig. 2. As our analysis focuses on cosmic filaments, we used DimIndex to extract structures that have a dimensionality of 1, that is, 1-dimensional structures. We depict the results of these three algorithms along projections on different planes in Fig. 2, with each row high-

Fig. 3. Results from MMCrawling on the filtered data. The distribution of galaxies in supergalactic coordinates (SGX, SGY, SGZ) is shown in black and the first iteration (N0) of MMCrawling is highlighted in purple on the *left* panel. Results from all nine iterations from MMCrawling are represented in various colours on the *right* panel. To visualise each iteration separately, see Appendix A.2.

lighting LAAT, EM3A, and DimIndex. We also provide a 3D visualisation of these results in Appendix A.1.

We then modelled the axes of the recovered structures using MMCrawling. This algorithm operates by randomly choosing a seed point that lies on the recovered central axes from the previous steps of 1-DREAM. It then crawls on both sides of the 1-dimensional manifold guided by the local PCA until it reaches the end of the filaments (refer to Canducci et al. 2022 for the definition used for determining the end of a filament).

The graph representing the first randomly chosen filament is then saved and the procedure is initiated again on the remaining number of galaxies, each time recovering an embedded graph object modelling the central axis of a given filament. The graphs as well as the galaxies that lie within neighbourhoods of size r centred on the nodes are catalogued. At the end of a complete MMCrawling run, we obtained a catalogue of graphs that model the central axis of the filaments within the data and for each graph, a set of galaxies that lie within a distance r from the corresponding filament core.
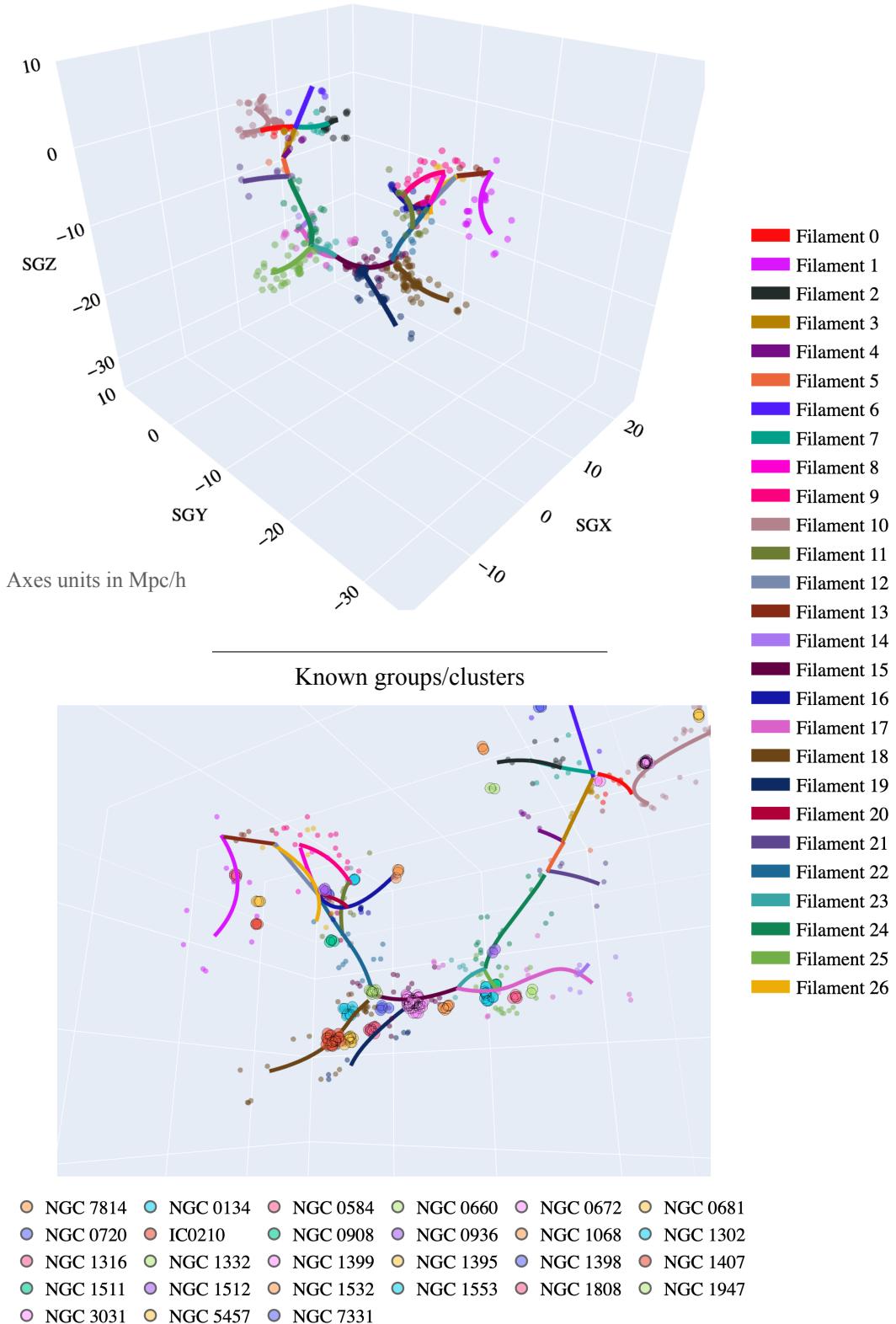
In terms of parameters, we adopted the same neighbourhood size of radius $r = 3$ Mpc/h and a distance between projected graph nodes of $\beta \times r = 1.5$ Mpc/h where $\beta = 0.5$. We chose the latter parameter to create the most reliable representations of the curvature of the filaments. Using a large β could lead to large jumps while crawling along the central axes to create the graphs and therefore, will not follow the length of the filaments smoothly, especially in regions where curvature is present. After applying MMCrawling once, we obtained a set of graphs which represent the modelled filaments shown in the left panel of Fig. 3. Awad et al. (2023) discussed the effect of the stochastic nature of this algorithm on its results and showed that differ-

ences occurring as a result of varying the random starting point of crawling is minimal but can become more likely when applied to filaments of low density. Therefore, given the sparsity of our observational data set, we expect to find differences in the modelled central axes when running MMCrawling several times (each time varying the randomly chosen starting position). To overcome this limitation and to ensure that the filaments we extracted were real and reliable, we ran Crawling numerous times until the graphs of the filaments we obtained overlapped with each other. Regions of overlapping graphs therefore indicate an agreement between the different runs and thus, point at reliable structures within the data. The resulting graphs from nine iterations are shown in Fig. 3 (right panel). We provide the separate results of each iteration in Appendix A.2).

We matched the coordinates of the nodes common between the graphs from all iterations. The segments connecting these nodes are further interpolated using cubic splines and then up-sampled to facilitate subsequent measurements such as the distances between the galaxies and their corresponding filament spine. The parameters mentioned in this sections are the only modified part from the suggested default-settings of all algorithms; these can be found in Table A.1. As we focus only on the filaments connected to the Fornax-Eridanus Complex, the filaments we present in this article pertain only to this region. Within this region, we detected 27 filaments, which we list in Table 1.

After up-sampling the modelled central axis for each retrieved filament, we repeated the search for galaxies near the identified cenral axes of filaments. For this, we used the `search_around_3D` function from Python's `astropy` module to find the nearest galaxies within a radius of 3 Mpc/h of each

Filaments around the Fornax-Eridanus Supercluster

Fig. 4. Filaments around the Fornax-Eridanus Complex. The distribution of galaxies belonging to 27 filament cores, displayed in supergalactic coordinates (SGX, SGY, SGZ), are represented in different colours on the *top* and *lower* panels. Each filament core is highlighted in the same colour as its member galaxies. Known groups/clusters from the group catalogues by Makarov & Karachentsev (2011) and Kourkchi & Tully (2017), which are part of the 27 filaments are also indicated in the *lower* panel.

Table 1. Filaments detected around the Fornax-Eridanus Complex

Filament name	Length of filament Mpc/*h*	N_{gal}	Known groups/ clusters
(1)	(2)	(3)	(4)
Filament 0	5.79	9	NGC 0672
Filament 1	4.73	24	IC 0210, NGC 0584, NGC 0681,
Filament 2	4.27	16	NGC 0660, NGC 7814
Filament 3	7.3	9	-
Filament 4	1.74	5	-
Filament 5	1.59	2	-
Filament 6	3.63	5	NGC 7331
Filament 7	4.69	5	-
Filament 8	1.5	6	NGC 0720
Filament 9	12.41	14	-
Filament 10	10.48	63	NGC 3031, NGC 5457
Filament 11	7.8	20	NGC 0134, NGC 0908
Filament 12	6.94	1	-
Filament 13	4.08	5	-
Filament 14	4.04	5	-
Filament 15	8.81	43	NGC 1398, NGC 1399, NGC 1532
Filament 16	6.08	12	NGC 1068
Filament 17	9.91	20	NGC 1808
Filament 18	7.95	76	NGC 1302, NGC 1332, NGC 1395, NGC 1407
Filament 19	5.95	50	NGC 1316, NGC 1399
Filament 20	3.52	7	NGC 0936
Filament 21	6.9	6	-
Filament 22	6.61	10	-
Filament 23	4.18	6	-
Filament 24	6.45	20	NGC 1512
Filament 25	10.35	41	NGC 1511, NGC 1553, NGC 1947
Filament 26	4.05	6	-

Notes. Column 1 – Filament identification number; Column 2 – Length of filament in Mpc/*h* ; Column 3 – Number of galaxies within $r = 3$ Mpc/*h* of the filament spine; Column 4 – Known groups/clusters from the group catalogues by Makarov & Karachentsev (2011) and Kourkchi & Tully (2017).

filament core. With this function, we also obtained the 3D Cartesian distance of each galaxy to its filament core.

4. Filaments around the Fornax-Eridanus Complex

In this section, we characterise the Fornax-Eridanus Complex by connecting our findings from 1-DREAM with known groups/clusters from the literature. We indicate the central axis of all 27 filaments and their member galaxies within our data cube in Fig. 4 (top panel). The number of galaxies within a neighbourhood radius of 3 Mpc/*h* of these filament cores is 486. Of the extracted subset at hand, 177 galaxies are located outside filaments (beyond 3 Mpc/*h* of the filament spines).
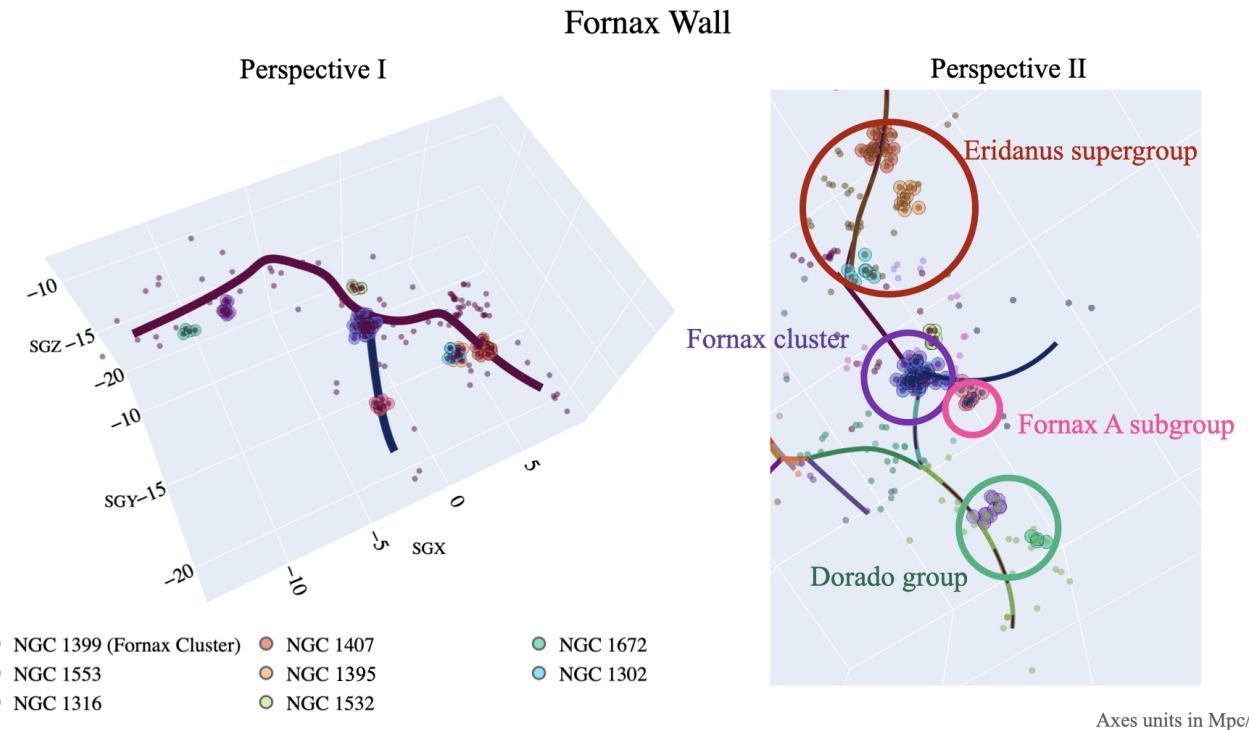
The filaments are connected to each other and form a coherent structure. This filamentary network is disconnected to filaments at the edge of the investigated volume. A possible explanation for this is the presence of fewer galaxies between filaments towards the edge and the filaments connected to the Fornax-Eridanus Complex. The remaining 270 galaxies from the extracted subset belong to these filaments that are not connected to the filamentary network around the Fornax cluster. In total, 81% of galaxies from our subset belong to filaments and 19% of galaxies are located outside filaments. We obtained the groups and clusters from the group catalogues by Makarov & Karachentsev (2011) and Kourkchi & Tully (2017) and indicate those that are located in our dataset, in the lower panel of Fig. 4.

Apart from groups and clusters within filaments, we find that ~30% of galaxies are isolated in filaments, that is, they are in *pristine filamentary* environments. With regard to the filaments around the Fornax-Eridanus Complex (486 galaxies), 33% of them are galaxies in *pristine filamentary* environments.

We estimated the length of the central axis of each filament, that is the embedded graph from its 3D Cartesian plane, and present these estimates in Table 1. The length of the filament-axes vary from 4 – 12 Mpc/*h*. The longest of them are the axis of Filament 12 ~ 12.41 Mpc/*h* comprising 14 galaxies and Filament 25 ~ 10.35 Mpc/*h* with 41 galaxies. We define filaments shorter than 5 Mpc/*h* as "minor filaments".

4.1. Known groups and clusters in filaments

The large-scale structure around the Fornax cluster amasses various filamentary environments. These filamentary environments are heterogeneous in nature, comprising galaxy groups, clusters, and pristine galaxies. Here, we detail this heterogeneity. We find that twenty out of twenty-seven filaments contain galaxy pairs, triplets, groups, and clusters; we list them in Table 1. As a reminder, we consider group and cluster galaxies as bound galaxies inside one virial radius (T16a). The most massive among these systems is the Fornax cluster (NGC 1399), located in Filament 15 and Filament 19. The latter filament connects the main Fornax cluster to its subgroup Fornax A (NGC 1316).

Fornax Wall

Fig. 5. Central axis of the Fornax Wall and its constituent galaxies. Two perspectives of the Fornax Wall are shown in each panel and all known groups/clusters are indicated in different colours. Perspective I (*left*) showcases the distribution of galaxies along the Fornax Wall as well as Filament 19, in supergalactic coordinates (SGX, SGY, SGZ), while Perspective II (*right*) is a snapshot of the same along the $x - y$ planes. The prominent structures – Fornax cluster, Fornax A subgroup, Eridanus supergroup, and the Dorado group are also indicated in Perspective II (*right*).

The NGC 1532 group is another system supposedly merging with the Fornax cluster and is part of Filament 19. The second most massive structure is the Eridanus supergroup (NGC 1302, NGC 1332, NGC 1395, NGC 1398, NGC 1407) and is part of two filaments, Filament 18 and Filament 15, extending from the Fornax cluster. The Dorado group (NGC 1553, NGC 1672) is connected to the Fornax cluster through Filament 23 and Filament 25.

An extension of the Southern Supercluster is the Cetus-Aries Cloud (NGC 0584, NGC 0681, NGC 0720, NGC 0908, NGC 0936, NGC 1068; see Tully 1987) and is connected to the Fornax-Eridanus Complex through Filament 22. Seven minor ($l < 5$ Mpc/h) filaments connect groups within the Cetus-Aries Cloud and some of these groups are located at intersecting nodes (NGC 0720, NGC 0936, NGC 1068). The Cetus I (NGC 1068) Cloud is part of Filament 16 while Cetus II (NGC 0584, NGC 0681) Cloud is part of Filament 1. Among these minor filaments, Filament 12 encompasses only one bright galaxy, and connects the Cetus II cloud to the NGC 0720 group through Filament 8 and to NGC 0908 group through Filament 22.

Known galaxy-groups within a distance of 10 Mpc from the Milky Way are NGC 0672, NGC 3031, NGC 5457 (see de Vaucouleurs 1975). The latter two are part of Filament 10, while NGC 0672 is part of Filament 0. These filaments are connected to Fornax and Dorado Clouds, through a series of filaments comprising mostly pristine galaxies and some galaxy-pairs; they are Filament 3, Filament 5, Filament 24.

Except for the aforementioned groups and clusters in the Fornax-Eridanus Complex, Cetus-Aries Clouds, and M31
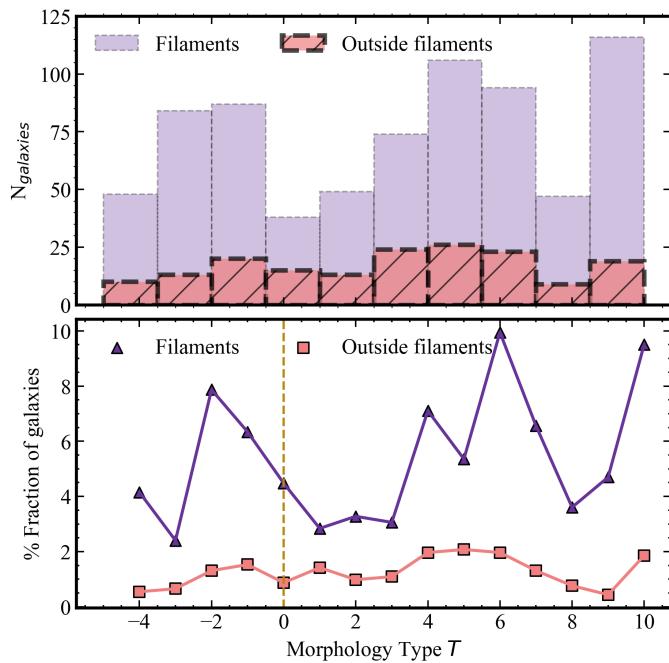
(NGC 3031) group, all other systems are pairs, triplets, and smaller groupings ($N_{gal} \leq 5$) of galaxies. Eleven filaments that we detect including the longest, that is, Filament 9, comprise only pristine galaxies (Filament 5, Filament 12, Filament 13, Filament 22, Filament 26), a few pairs (Filament 4, Filament 9, Filament 14, Filament 21), and triplets (Filament 4, Filament 23)[5]. On the whole, the large-scale structure around the Fornax cluster we detected encompasses various filamentary environments.

4.2. The Fornax Wall

The Fornax Wall was first discovered by Fairall et al. (1994) and the Fornax-Eridanus supercluster is embedded within it. Fairall et al. (1994) described *Great Walls* as a large concentration of galaxies in a volume of several thousand km s^{-1} in redshift space.

We identified the central axis of this structure that appeared six out of nine iterations with MMCrawling. The four filamentary segments that together constitute this topological feature are Filament 15, Filament 18, Filament 23, and Filament 25. We show two perspectives of the Fornax Wall in Fig. 5 and indicate all the major groups and clusters (Dorado group, Fornax cluster and its subgroup – Fornax A, Eridanus supergroup) in this region. We also indicate Filament 19 (length ∼ 6 Mpc/h) which connects the Fornax cluster to its subgroup Fornax A. We

---

[5] Table 1 shows only the known groups/clusters from the group catalogues by Makarov & Karachentsev (2011) and Kourkchi & Tully (2017). However, some filaments contain more groups. For example, based on the catalogue by T16a, Filament 3 contains a group with $N_{gal} = 5$, but is not tabulated here.

Fig. 6. Histogram of galaxy-morphology in filaments and outside filaments. *Top panel*: Purple indicates galaxies within filaments and coral dashed histogram indicates galaxies outside filaments. *Lower panel*: Purple triangles represent galaxies in filaments and coral squares represent those outside filaments. Yellow dashed line at $T = 0$ indicates the separation between ETGs and LTGs.
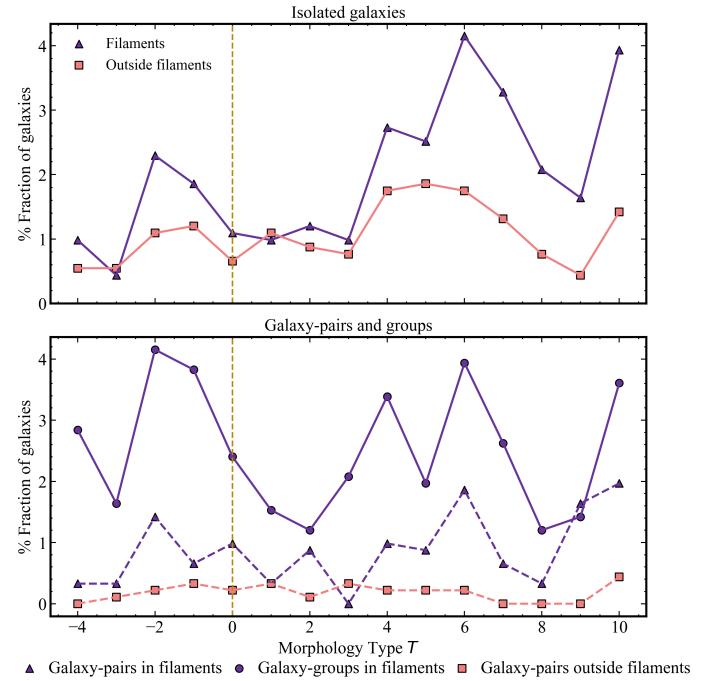
estimated the length of the central axis of this structure to be 31 Mpc/h and it hosts 216 galaxies with $\log_{10}(M_*/M_\odot) > 8.45$ within a neighbourhood radius of 3 Mpc/h.

With 1-DREAM, the Fornax Wall was detected as a 1-dimensional feature and not as a 2-dimensional one as intuitively expected for cosmic walls. While the literature has identified this structure to be a cosmic wall, further analysis is required to comprehend the nature of it. We speculate that the structure we identified could be a filament embedded in a wall. In a forthcoming article (Raj et al. in prep), we will discuss this in detail.

5. Morphology-density relation of galaxies in filaments

In this section, we investigate the morphology-density relation of galaxies in the large-scale structure around the Fornax-Eridanus Complex with particular emphasis on galaxies part of the Fornax Wall. To do this, we segregate the catalogue into two main classes of galaxy morphology, defined by their Morphology Type T (obtained from Kourkchi & Tully 2017 [6]); they are early-type galaxies (ETGs, $-6 \leq T \leq 0$) and late-type galaxies (LTGs, $T > 0$). Of the extracted subset, 69% are LTGs and 31% are ETGs. First, we investigate the effect of the cosmic environment on galaxy-morphology; the two cosmic environments are *filaments* and *outside filaments* (beyond 3 Mpc/h of the filament spine). We show this in Fig. 6 and tabulate them in Table 2. In the top panel of Fig. 6, we present the numbers of galaxies within each Morphology Type T bin for both cosmic environments (filaments and outside them). We also present the percentage fraction

Fig. 7. Histogram of galaxy-morphology in different environments. In both panels, we show the percentage fraction of T-Type with regard to the total galaxy population, and we indicate the separation between ETGs and LTGs with a yellow dashed line, that is, at $T = 0$; *Top panel*: purple triangles indicate galaxies in pristine filamentary environments and coral squares indicate those outside filaments; *Lower panel*: purple triangles (*solid lines*) indicate galaxy-pairs in filaments, purple circles (*dashed lines*) indicate galaxy-groups in filaments, and coral squares indicate galaxy-pairs outside filaments.

for the same in the lower panel, where we normalise our counts such that the sum of all points within this panel equals 100%. As mentioned in Sect. 4, ~ 19% of galaxies in our subset are located outside filaments. Among the galaxies outside filaments, 27% of them are ETGs and 73% are LTGs. In Fig. 7, we also indicate the environments within which these galaxies are located (*isolated*, *pairs*, *groups*). Similarly, all percentages in each panel of this Figure sum to 100%. The fraction of ETGs outside filaments are mostly isolated (top panel of Fig. 7) and < 1% of the subset is ETGs in galaxy-pairs (lower panel of Fig. 7).
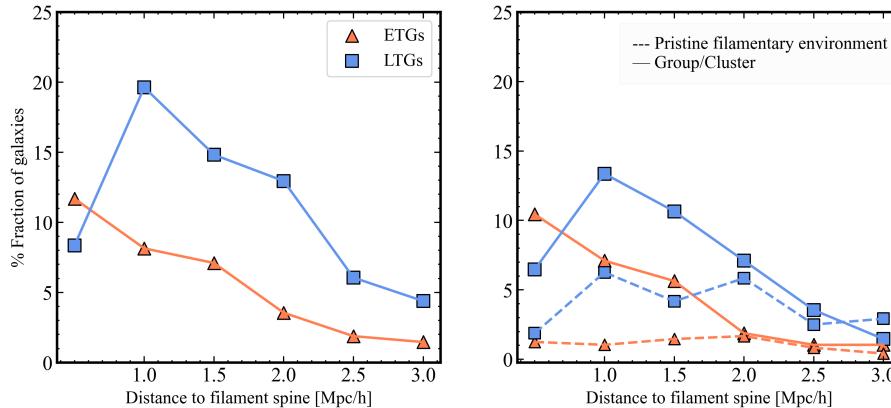
We do not find any groups ($N_{gal} > 2$) outside filaments. On the other hand, the fraction of ETGs is the highest in groups/clusters (15%) within filaments. Concerning LTGs in filaments, we find that their fraction (with regard to the subset) is the same in pristine filamentary environments (top panel of Fig. 7) and groups/clusters (lower panel of Fig. 7), which is ~ 23% . We speculate that the galaxies outside filaments could belong to voids and a detailed study of this will be presented in a forthcoming article (Raj et al. in prep). From the literature (e.g. Cautun et al. 2014a; Awad et al. 2023), the number density of galaxies in voids is lowest among other cosmic environments.

Now, we examine the role of galaxies' proximity to the filament core on their morphology. We determine the fraction of each morphology class with respect to the entire population of filament galaxies (from Table 1), in bins of 0.5 Mpc/h from the filament core (we tabulate the number of galaxies in their respective bins in Table A.2). In Fig. 8 (left panel), we show that the fraction of the ETG-population decreases with distance to the filament and 27% of filament galaxies are ETGs in groups/clusters

Table 2. Galaxy population in cosmic environments

Morphology	Filaments % fraction			Outside filaments % fraction		
	Groups	Pristine	galaxy-pairs	Groups	Isolated	galaxy-pairs
(1)		(2)			(3)	
ETG	15	7	4	–	5	< 1
LTG	23	23	9	–	12	2

Notes. Column 1 – Morphology class; Column 2 – Percentage fraction of galaxies in filaments, of which belong to groups/clusters, pristine environments, and galaxy-pairs; Column 3 – Percentage fraction of galaxies outside filaments, of which belong to groups/clusters, isolated environments, and galaxy-pairs.

Fig. 8. Morphology of galaxies in filaments around the Fornax-Eridanus Complex. In both panels, we show a histogram of ETGs (*orange triangles*) and LTGs (*blue squares*) as a function of their distance to the filament spine. In the *right* panel, the dataset is divided in two categories, pristine filamentary galaxies (*dashed lines*) and those associated to groups/clusters (*solid line*).

(see right panel of Fig. 8). The fraction of the LTG-population ($\sim 8\%$) is lower than that of the ETG-population ($\sim 12\%$) at 0.5 Mpc from the filament spine. However, at 1 Mpc/h from the filament spine, the LTG-population increases to 20% (see left panel of Fig. 8). Upon further inspection of this increment (at 1 Mpc), 13% of these LTGs are in groups/clusters and 7% are in pristine filamentary environments. We attribute this increment to LTGs which could be in outskirts of groups/clusters (see right panel of Fig. 8) or to triplets/pairs. Of the total filament-population around the Fornax-Eridanus Complex, we find that 7% are ETGs and 24% are LTGs in pristine filamentary environments (see right panel of Fig. 8), 27% are ETGs are 42% are LTGs in groups/clusters within filaments (refer to Table A.2). We also investigate the role of the filament number-density on the morphology of galaxies. In Fig. 9 (top panel), we indicate that longer filaments have more galaxies than their shorter counterparts. From this, we estimate the number-density of each filament and indicate this with a colour bar in Fig. 9 (top panel). The densest filaments include Filament 15, Filament 18, Filament 23, Filament 25, which together form the central axis of the Fornax Wall. In Fig. 9, we find that the fraction of ETGs (lower left panel) increases with the density of their hosting filament, while that of LTGs (lower right panel) decreases with increasing density of their filaments. This correlation indicates the effect of the local environment on morphology of galaxies, as proposed by Dressler (1980).

Now we explain the effect of the large-scale environment on the morphology of galaxies part of the Fornax Wall. In the top-left panel of Fig. 10, we show the 3D projection of the central axis of the Fornax Wall and indicate the Morphological Type T of each galaxy in the colour bar. We also implemented a cross-sectional view along the Fornax Wall to inspect the distribution of galaxies surrounding its centre. The procedure explained be-
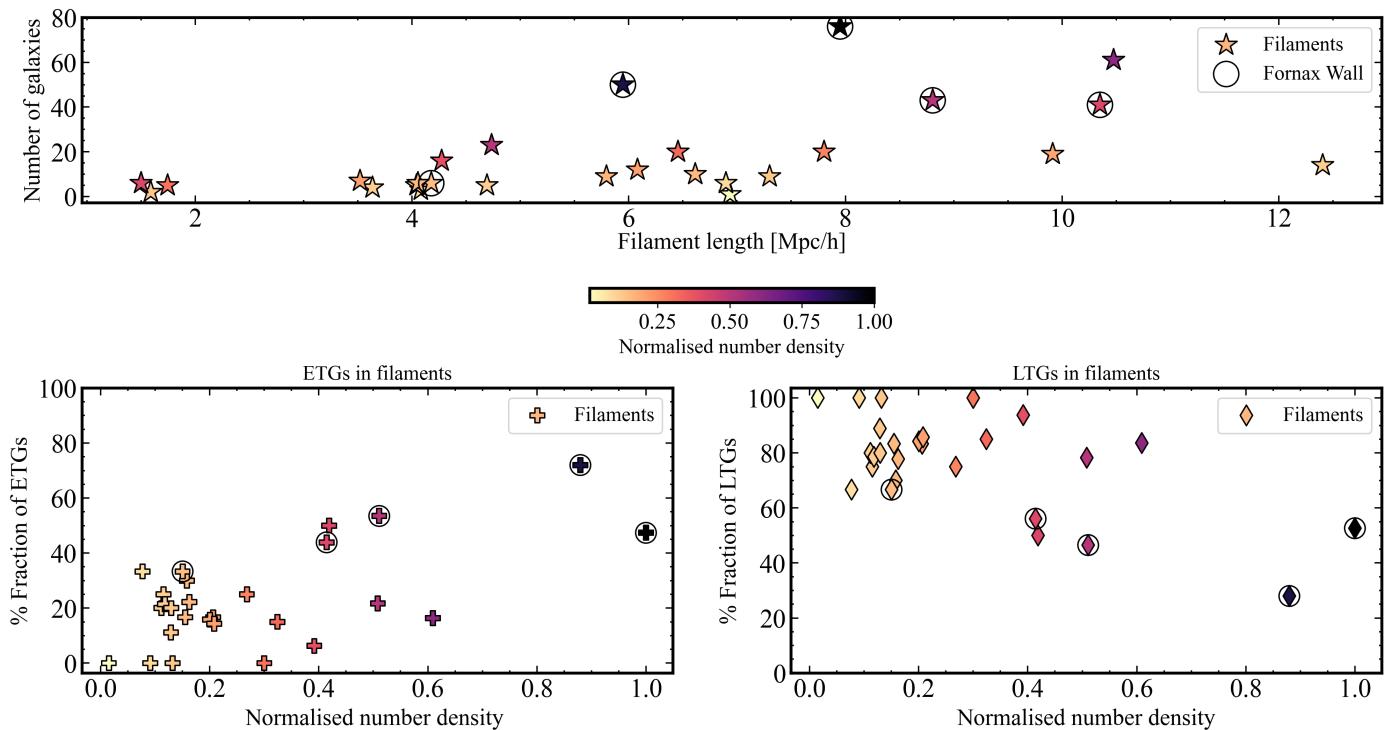
low was developed by (Canducci et al. 2022) and is briefly recounted here. With this aim, we constructed a series of orthonormal coordinate frames centred on the spine of the Wall and co-moving along its length. For every segment $\hat{\xi}_i = \frac{1}{|\xi_i|}(\xi_i^1, \xi_i^2, \xi_i^3)$ connecting two points that sample the Fornax Wall's central axis, we recovered two vectors $\boldsymbol{v}_1 = (v_1^1, v_1^2, v_1^3)$ and $\boldsymbol{v}_2 = (v_2^1, v_2^2, v_2^3)$ that are orthogonal to $\hat{\xi}_i$ and that span the perpendicular plane to the axis of the Fornax Wall at the given point i. For finding these vectors, the following system of linear equations is solved:

$$\begin{cases} \boldsymbol{v}_1 \cdot \boldsymbol{v}_2 = v_1^1 v_2^1 + v_1^2 v_2^2 + v_1^3 v_2^3 \\ \boldsymbol{v}_1 \cdot \hat{\xi}_i = v_1^1 \hat{\xi}_i^1 + v_1^2 \hat{\xi}_i^2 + v_1^3 \hat{\xi}_i^3 \\ \boldsymbol{v}_2 \cdot \hat{\xi}_i = v_2^1 \hat{\xi}_i^1 + v_2^2 \hat{\xi}_i^2 + v_2^3 \hat{\xi}_i^3. \end{cases} \quad (1)$$

This system of equations is degenerate and therefore permits an infinite number of solutions. Therefore, to keep a consistent orientation along the length of the central axis, we fixed the solution to be of the form:

$$\boldsymbol{v}_1 = (\hat{\xi}_i^2, -\hat{\xi}_i^1, 0), \qquad \boldsymbol{v}_2 = (\hat{\xi}_i^1 \hat{\xi}_i^3, \hat{\xi}_i^2 \hat{\xi}_i^3, -(\hat{\xi}_i^1)^2 - (\hat{\xi}_i^2)^2). \quad (2)$$

The retrieved vectors are then normalised and are shown for every point on the central axis (top right panel of Fig. 10). As mentioned, these vectors span the orthogonal plane to the axis at each given point i. Finally, we project the positions of the galaxies belonging to the Fornax Wall onto the orthogonal plane centred on the nearest point on the axis to each galaxy. These projected positions are then stacked to achieve the final cross-sectional view of all galaxies belonging to the Fornax Wall within a distance of 3 Mpc/h to its centre. We show this result in the lower left panel of Fig. 10, where the galaxies are also coloured by their Morphology Type T.

Fig. 9. Morphology-density relation of galaxies in filaments around the Fornax-Eridanus Complex. *Top panel*: Length of each filament (*stars*) versus the number of galaxies belonging to it. For all panels, the colour bar indicates the normalised galaxy number-density of each filament (N_{gal}/l), and *circles* highlight filaments that constitute the Fornax Wall (includes Filament 19); *Lower left panel*: Normalised galaxy number-density versus the percentage fraction of ETGs in each filament, represented by crosses; *Lower right panel*: Same as the *lower left panel*, but for LTGs. Here, each diamond represents a filament.

Similar to our results on the morphology-density relation of galaxies in filaments, we also see a morphological segregation of galaxies in the large-scale environment of the Fornax Wall. We find that ∼ 44% (216) of galaxies which belong to the filamentary network of our data subset (486 galaxies) are associated to the Fornax Wall. In the lower-right panel of Fig. 10, we see that the fraction of the LTG-population (7%) is lower than that of ETGs (13%) near the central axis of the filament ∼ 0.5 Mpc/*h*. However, at 1 Mpc, the fraction of LTGs increases to 13% and at 1.5 Mpc, the fraction of LTGs is similar to that of ETGs (11%). Beyond this radius, the fraction of LTGs is higher than of that ETGs.

From Fig. 10, we can also see that the galaxy-number density of the Fornax Wall is larger within its centre (point (0, 0) in the lower left panel) and decreases gradually as we move radially away from it. This drop in the density of cosmic filaments as we move radially away from their centres has been shown previously in the form of radial density profiles of simulated cosmic filaments (Ramsøy et al. 2021; Pfeifer et al. 2022; Galárraga-Espinosa et al. 2023; Awad et al. 2023). Therefore, we observe the same correlation between density and distance away from the centre of the Fornax Wall.

Kuchner et al. (2022) showed that filament environments can vary in number-density and type (pristine or groups/cluster). Likewise, the galaxy-number density could vary across galaxy walls, owing to some of them within group/cluster or pristine environments. This number-density would imply different local environments across a filament/wall. Here, we explore the different environments across the Fornax Wall and its impact on its member galaxies. We do this by dividing the Wall into 10 segments (length 2.4–3.8 Mpc/*h*) and then estimate the volume and
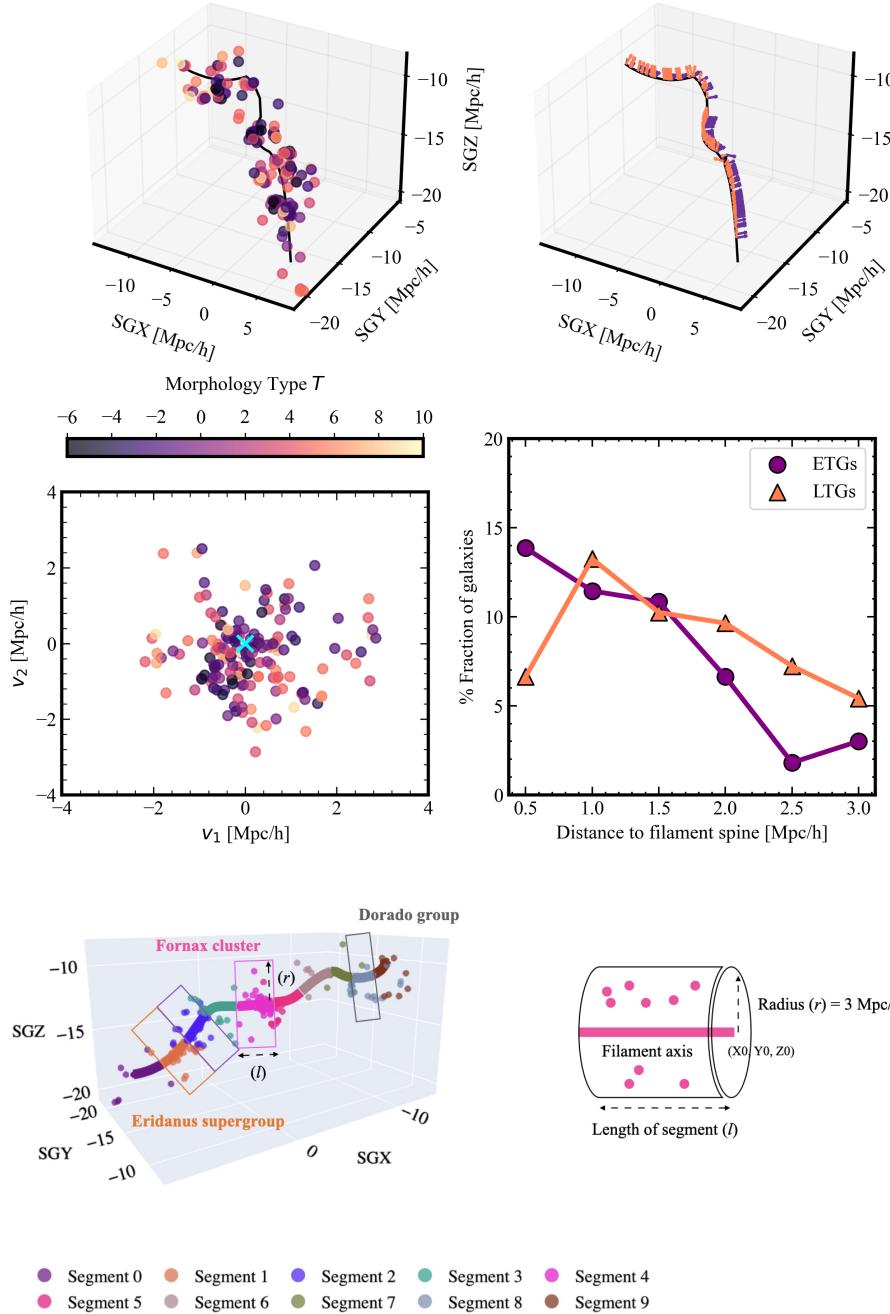
density of each segment. In Fig. 11, we illustrate the segments and indicate the major clusters within the the Fornax Wall.

We show the results of this analysis in Fig. 12. Here, we describe each panel of this figure. In the top panel, we plot the number density of each segment (left) and their population number (right), and find that the density peaks in segments containing the Eridanus supergroup, Fornax cluster, and the Dorado group. In the middle panel, we plot the percentage fraction of ETGs (left) and LTGs (right), and find that ETGs populate the densest regions of the Fornax Wall. Within the Eridanus supergroup, the NGC 1407 group is the most dynamically evolved (located in segment 1; Brough et al. 2006) and 75% of its galaxies are early-type and 25 % are late-type; this is similar to the Fornax cluster. On the contrary, the region of this supergroup which comprises NGC 1395 (segment 2) has more (60%) LTGs than ETGs. Lastly, the Dorado group has 60% ETGs and 40% LTGs. To support the argument that ETGs populate the densest regions of the Fornax Wall, we illustrate the galaxy number density in the lower panel of Fig. 12.
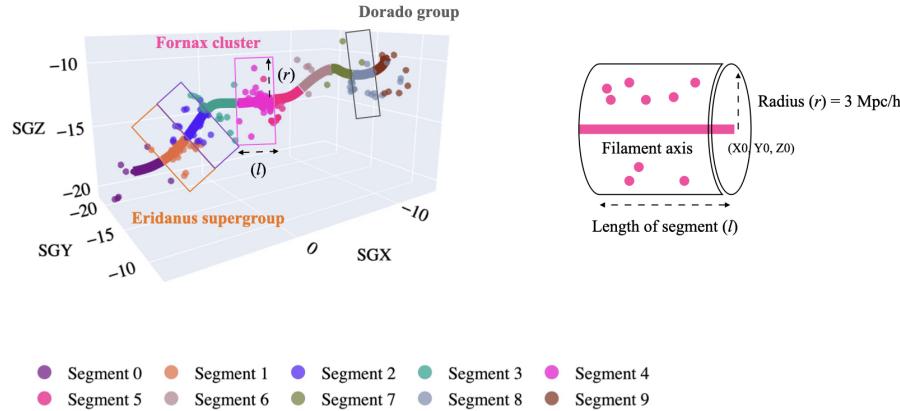
6. Large-scale environment around the Fornax-Eridanus Complex

In this section, we compare our results to previous findings thereby investigating the role of the large-scale environment surrounding the Fornax-Eridanus Complex on its constituent galaxies. With this, we also show the extent of the detected filaments in the Cosmic Web.

Over-densities in *Great Walls* have been attributed to cores within superclusters embedded in them (Einasto et al. 2016).

Fig. 10. Morphology of galaxies and cross-sectional view of the Fornax Wall. *Top left panel*: 3D view of the Fornax Wall in super-galactic coordinates. Each galaxy is highlighted by its Morphology Type T, as shown on the colour bar; *Top right panel*: Normalised vectors for every galaxy on the central axis of the Fornax Wall in coral and purple; *Lower left panel*: Cross-sectional view of all galaxies belonging to the Fornax Wall within a distance of 3 Mpc/h to its centre. The centre is marked with a cyan cross and the galaxies are denoted by their Morphology Type T, as shown in the colour bar. *Lower right panel*: Histogram of the ETGs (*purple circles*) and LTGs (*orange triangles*) as a function of their distance to the Fornax Wall.

Fig. 11. Segments of the Fornax Wall. *Left panel*: Distribution of galaxies part of the Fornax Wall, represented in supergalactic coordinates (SGX, SGY, SGZ). The Fornax Wall is divided into ten segments and each segment is highlighted with a different colour. The windows indicate the location of the major systems – Eridanus supergroup, Fornax cluster, and Dorado group in their respective segments. *Right panel*: Illustration of the method for estimating the length, radius, and volume of a segment's cylinder.
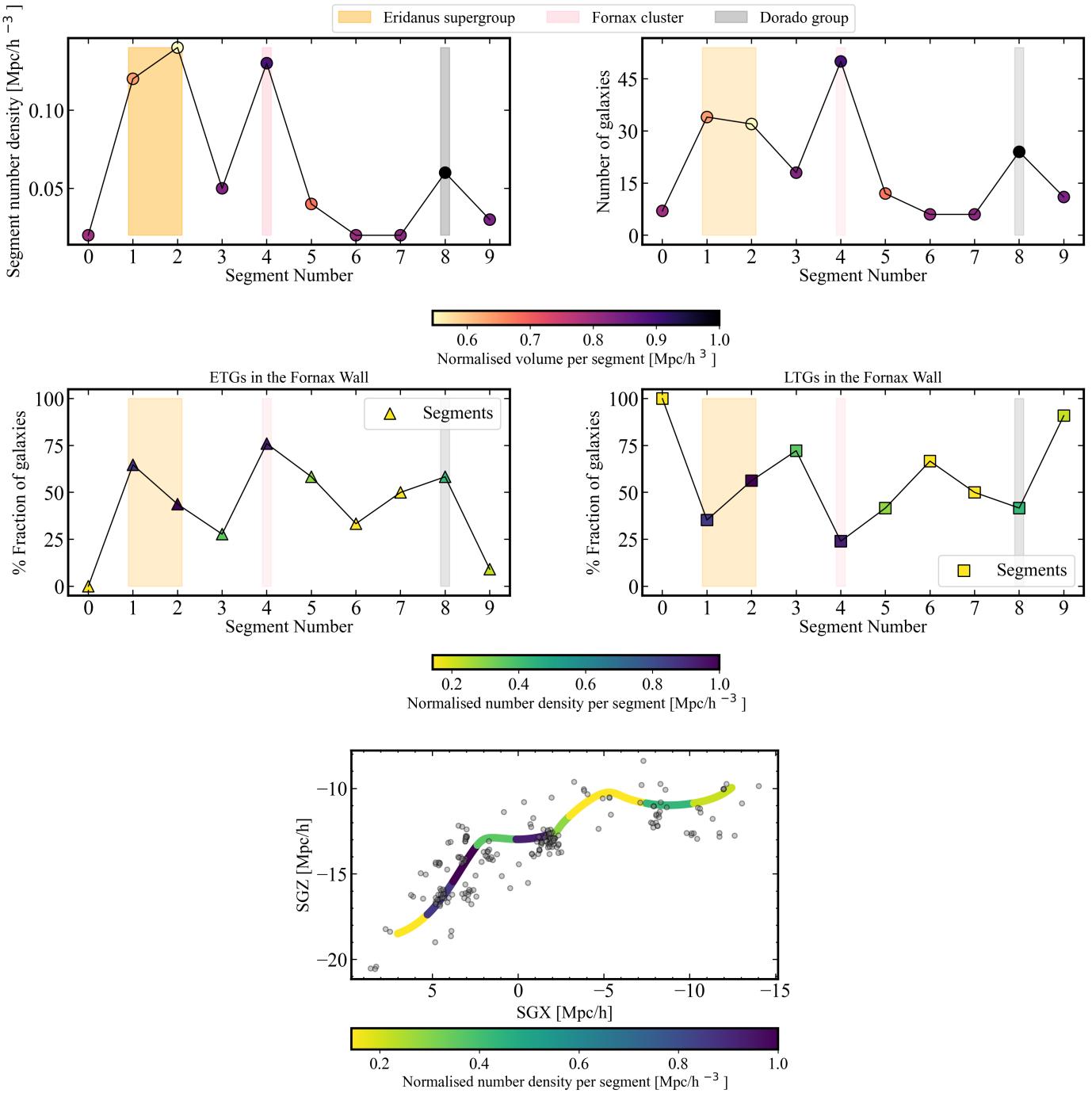
Gravitational instability theory (Zel'dovich 1970; Icke 1973; White & Silk 1979) is the main contributor of the flow of matter within the Universe. This flow occurs from lower-density regions such as voids to higher-density regions such as walls. In this context, it is worth noting the presence of any cosmic voids surrounding the Fornax Wall which could play a role in shaping its structure.

Using the Nexus+ methodology, Cautun et al. (2014b) demonstrated this mode of matter transfer within the Millennium Simulations (Springel 2005; Boylan-Kolchin et al. 2009) evolved from redshift $z = 2$ till the present. They also showed that any transport of mass that defies this rule is an artefact of the method used for structure-identification and thus does not challenge the underlying cosmological evolution theories. Cautun et al. (2014b) also emphasised the strong outflow that occurs from voids towards sheets which act as void boundaries. As in-

dicated by Jones & Jones (1980); Phillipps & Davies (1992); Drinkwater et al. (2000), a large void extending around 40 Mpc exists immediately beyond the Fornax cluster. The close presence of this void therefore fortifies the claim of the existence of a cosmic structure at its boundary (i.e. the Fornax Wall). It also suggests that many of the galaxies within the Fornax Wall have been the result of outflow occurring between the two environments. It is possible to verify this claim by looking at the dynamical behaviour of the galaxies within the wall and comparing the direction with which they are moving with respect to the Fornax Void. We leave such explorations for future work.
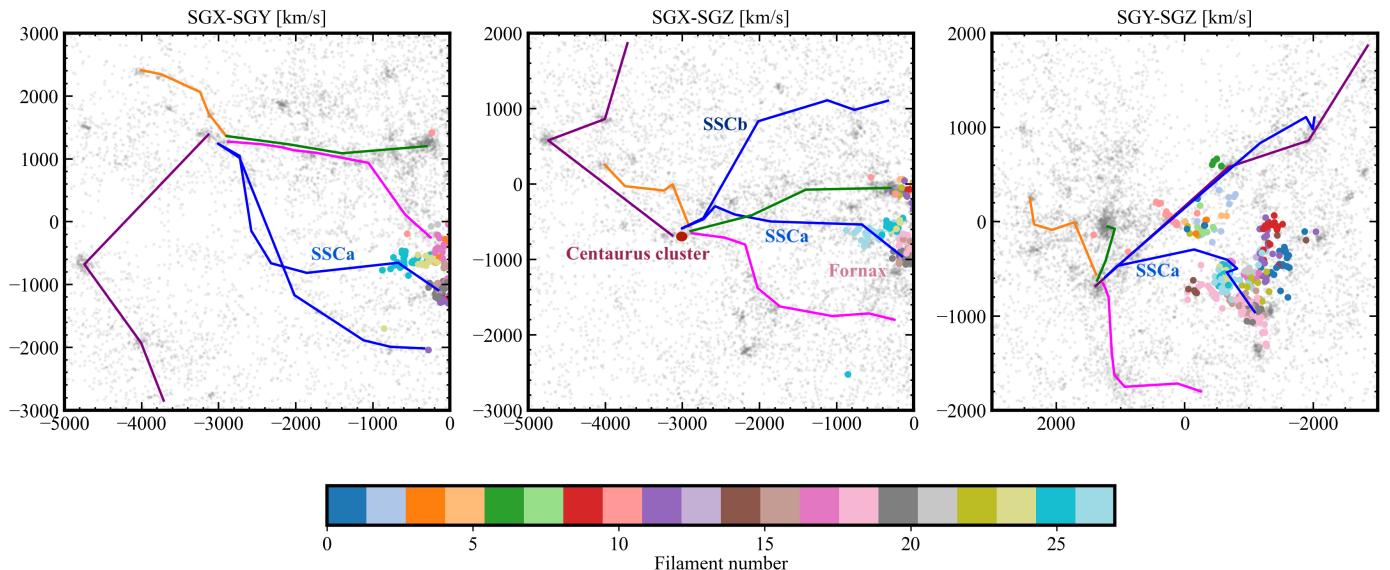
Our analysis reveals a significant morphological segregation of ETGs dominating dense environments such as dynamically evolved groups/clusters of filaments. In fact, the ETG population decreases with increasing distance to the filament spine. Moreover, groups and clusters in the high-density core of the Fornax-

Fig. 12. Morphology-density relation of galaxies part of the Fornax Wall. *Top panel*: In both panels, *x*-axes represent the segment number corresponding to Fig. 11 and *y*-axis represents the segment number density on the *left* and number of galaxies on the *right* panel. The colour bar indicates the normalised volume per segment. The major systems as indicated in Fig. 11 are also highlighted here– Eridanus supergroup in orange, Fornax cluster in pink, and Dorado group in grey; *Middle panel*: Fraction of ETGs (*left*) and LTGs (*right*) in each segment. The colour bar indicates the normalised number density per segment; *Lower panel*: The Fornax Wall and its constituent galaxies, projected in the supergalactic *x-z* plane. Each segment is coloured according to its density; the colour bar depicts the normalised density.

Eridanus Complex are more ETG-rich than other environments in filaments connecting to the Complex. There has been evidence of the effect of the large-scale environment on galaxy properties, such that the core of superclusters are populated with red galaxies, while blue galaxies are homogeneously distributed in the outskirts of superclusters (see Haines et al. 2006; Einasto et al. 2011b, 2018, 2022). A morphological-segregation in superclusters can also be attributed to its evolutionary history (Einasto et al. 1980). In the case of the Fornax-Eridanus Complex, the merging of groups within it, further suggests that pre-processing of galaxies before cluster-infall is the dominating factor for the observed morphological segregation. Moreover, filaments outside the Complex have lower fractions of ETGs, which are mostly located in groups near the central axis of filaments.

Fig. 13. Cosmic web around the Fornax-Eridanus Complex. The V8k catalogue is over-plotted here (*grey dots*) to show the extension of our detected filaments. Galaxies part of our dataset are highlighted with different colours based on their filament-membership; this is shown in the colour bar. The five filaments spines feeding the Centaurs cluster, as depicted by Courtois et al. (2013), are plotted here. Among them, the two branches of the Southern Supercluster Strand– SSCa and SSCb, the Centaurus cluster, and the Fornax cluster are also marked in the centre panel. Each panel is projected in supergalactic coordinates along *x-y*, *x-z*, and *y-z* planes.

Filaments are considered to be an intermediate-density region and follow the morphology-density relation (e.g Kuutma et al. 2017; Santiago-Bautista et al. 2020; Hoosain et al. 2024). However, we suspect that the local density might not be the only factor contributing to a galaxy's morphology. An example of this is Filament 10, where the M81 group is located. Although this filament ($l \sim 10.5$ Mpc/h) has 63 galaxies, both in groups and pristine environments, the fraction of LTGs (85%) is higher than that of ETGs (15%). We speculate that another possible contributing factor to a galaxy's morphology could be its proximity to a filament core. As most of the galaxies in the M81 group are beyond 1.5 Mpc/h from the central axis of the filament, the primordial gas supply from the Cosmic Web (see Aragon Calvo et al. 2019; Winkel et al. 2021) might not be completely shut down. A combination of several internal and external processes (e.g. ram-pressure stripping; Gunn & Gott 1972) in galaxy-clusters can eventually diminish the gas content in galaxies.

The large-scale structure around the Fornax-Eridanus Complex constitutes a variety of filamentary environments, not only in terms of galaxy number-density, but also its evolutionary history. Previously, Kuchner et al. (2022) demonstrated the heterogeneity of filamentary environments such that the filaments can be pristine or dominated by groups/clusters. In order to examine the effect of the filament itself on galaxy properties, the groups/clusters within it have to be excluded. We elucidated this in Fig. 8 (right panel) and found $\sim 7\%$ of the galaxy-population in filaments are ETGs in pristine environments. On the other hand, the fraction of the LTG-population ($\sim 24\%$) in pristine environments of filaments is higher than that of ETGs. Further exploration of the stellar mass and gas content of these galaxies is required to understand the formation channels of ETGs in pristine environments of filaments.

Courtois et al. (2013) showed that five filaments emerge from the Centaurus cluster, with one of them connected to the Southern Supercluster Strand SSCa (Fornax-Eridanus-Dorado). In or-

der to visualise the extent of the emerging filament SSCa and its connection to the filaments we detect, we plot them in Fig. 13 [7]. Filament 25 is part of the Fornax Wall, and an extension of this filament constitutes SSCa, that connects to the Centaurs cluster. While the Fornax Wall itself has no clear boundary, the density contrast from this structure to its nearby filaments would suggest a filamentary network of lower galaxy number-density, that continues all the way to the Centaurus cluster. The other branch of the Southern Supercluster Strand is SSCb, which is also one of the emerging filaments from the Centaurus cluster (see Fig. 13). This branch is connected to the Fornax-Eridanus Complex through the Cetus-Aries Cloud (Tully & Fisher 1987). Although, Tully & Fisher (1987) indicated that the Cetus-Aries Cloud is a minor filament, our results reveal that several small filaments connect groups within this Cloud, as explained in Sect. 4.1.

7. Summary and Conclusions

In this work, we explored the Fornax-Eridanus Complex using the novel ML toolbox, 1-DREAM. We then presented the analysis of the filamentary network that we detected within the region. This analysis included an investigation of the influence of filamentary environments on the morphology of galaxies, defined by the Morphological Type T parameter. Finally, we discussed the large-scale environment around the Fornax-Eridanus Complex. We enumerate the main results of this study below:

1. With 1-DREAM, we identified a filamentary network of galaxies around the Fornax-Eridanus Complex. Of the extracted volume, 81% are galaxies located in filaments and 19% are galaxies outside filaments. The filamentary network around the Fornax-Eridanus Complex comprises 27 filaments that vary in length and galaxy number-density. These

---

[7] We matched the subset of the T16a dataset to the V8k catalogue from EDD (Tully et al. 2009) and this resulted in 386 out of 486 galaxies.

filaments exhibit various environments, which are defined by their number-density and groups/clusters embedded in them. Among them, some contain only pristine filament galaxies.

2. The subsequent analysis of the aforementioned filaments revealed a well-known structure– the Fornax Wall, which encompasses the Fornax-Eridanus-Dorado supercluster. The length of the central axis of this Wall is ~ 31 Mpc/h and hosts 216 galaxies with $\log_{10}(M_*/M_\odot) > 8.45$ within a neighbourhood radius of 3 Mpc/h.

3. The literature suggests that the morphology-density relation of galaxies extends to both filaments and walls. Our analysis corroborates this by showing a decrease in the fraction of the ETG-population ($-6 \leq T \leq 0$) with increasing distances from the filament spine. The fraction of the LTG-population ($T > 0$; 8%) in our catalogue is lower than that of ETGs (12%) at 0.5 Mpc from the filament spine. We attribute the increment (20%) at 1 Mpc/h to LTGs located in the outskirts of groups/clusters as well as galaxy-triplets/pairs. Of the total galaxy-population in filaments around the Fornax-Eridanus Complex, $\sim 27\%$ are ETGs and $\sim 42\%$ are LTGs in groups/clusters within filaments, while $\sim 7\%$ are ETGs and $\sim 24\%$ are LTGs located in pristine environments of filaments. Further investigation of the gas content and stellar mass of ETGs is required to understand their formation channels in pristine environments.

4. We observed that 44% of the galaxies from the filamentary network belong to the Fornax Wall. Our findings show that the galaxy number-density varies across the Fornax Wall and therefore impacts its member-galaxies differently. As such, ETGs dominate the densest regions of the Fornax Wall.

In conclusion, this study has revealed the Cosmic Web around the Fornax cluster, displaying various filamentary environments within and around the supercluster. With this, our research reaffirms the heterogeneity of filamentary environments that was proposed by Kuchner et al. (2022). When investigating the impact of the local environment on galaxy morphology, number-density as well as proximity to the filament core (central axis) are to be considered. In this context, the morphological segregation in the Fornax Wall can be attributed to pre-processing in groups embedded in it and the inflow of galaxies from the surrounding Fornax Void. Lastly, we restate that 1-DREAM is a reliable ML tool to model the central axis of filaments, which in turn is essential to study the role of the environment on galaxy properties. As such, our future endeavours entail an in-depth study of the structure of the Fornax Wall as well as some observational properties of different galaxy populations pertaining to the filaments we analysed here.

References

Aghanim, N., Tuominen, T., Bonjean, V., et al. 2024, arXiv e-prints, arXiv:2402.18455

Aragón-Calvo, M. A., Jones, B. J. T., van de Weygaert, R., & van der Hulst, J. M. 2007, A&A, 474, 315

Aragon Calvo, M. A., Neyrinck, M. C., & Silk, J. 2019, The Open Journal of Astrophysics, 2, 7

Araya-Melo, P. A., Reisenegger, A., Meza, A., et al. 2009, MNRAS, 399, 97

Astropy Collaboration, Price-Whelan, A. M., Lim, P. L., et al. 2022, ApJ, 935, 167

Astropy Collaboration, Price-Whelan, A. M., Sipőcz, B. M., et al. 2018, AJ, 156, 123

Astropy Collaboration, Robitaille, T. P., Tollerud, E. J., et al. 2013, A&A, 558, A33

Awad, P., Peletier, R., Canducci, M., et al. 2023, MNRAS, 520, 4517

Bag, S., Liivamägi, L. J., & Einasto, M. 2023, MNRAS, 521, 4712

Balogh, M. L., Navarro, J. F., & Morris, S. L. 2000, ApJ, 540, 113

Bamford, S. P., Nichol, R. C., Baldry, I. K., et al. 2009, MNRAS, 393, 1324

Benavides, J. A., Sales, L. V., Abadi, M. G., et al. 2023, MNRAS, 522, 1033

Bidaran, B., La Barbera, F., Pasquali, A., et al. 2022, MNRAS, 515, 4622

Bond, J. R., Kofman, L., & Pogosyan, D. 1996, Nature, 380, 603

Bonnaire, T., Aghanim, N., Decelle, A., & Douspis, M. 2020, A&A, 637, A18

Boselli, A. & Gavazzi, G. 2006, PASP, 118, 517

Boylan-Kolchin, M., Springel, V., White, S. D. M., Jenkins, A., & Lemson, G. 2009, MNRAS, 398, 1150

Brough, S., Forbes, D. A., Kilborn, V. A., Couch, W., & Colless, M. 2006, MNRAS, 369, 1351

Brown, T., Roberts, I. D., Thorp, M., et al. 2023, ApJ, 956, 37

Bulichi, T.-E., Dave, R., & Kraljic, K. 2023, arXiv e-prints, arXiv:2309.03282

Canducci, M., Awad, P., Taghribi, A., et al. 2022, Astronomy and Computing, 41, 100658

Canducci, M., Tiño, P., & Mastropietro, M. 2022, Artificial Intelligence, 302, 103579

Castignani, G., Combes, F., Jablonka, P., et al. 2022, A&A, 657, A9

Cautun, M., van de Weygaert, R., & Jones, B. J. T. 2013a, MNRAS, 429, 1286

Cautun, M., van de Weygaert, R., & Jones, B. J. T. 2013b, MNRAS, 429, 1286

Cautun, M., van de Weygaert, R., Jones, B. J. T., & Frenk, C. S. 2014a, MNRAS, 441, 2923

Cautun, M., van de Weygaert, R., Jones, B. J. T., & Frenk, C. S. 2014b, MNRAS, 441, 2923

Chen, Y.-C., Ho, S., Mandelbaum, R., et al. 2017, MNRAS, 466, 1880

Chon, G., Böhringer, H., Collins, C. A., & Krause, M. 2014, A&A, 567, A144

Chung, J., Kim, S., Rey, S.-C., & Lee, Y. 2021, ApJ, 923, 235

Colless, M., Dalton, G., Maddox, S., et al. 2001, MNRAS, 328, 1039

Cornwell, D. J., Kuchner, U., Gray, M. E., et al. 2024, MNRAS, 527, 23

Courtois, H. M., Pomarède, D., Tully, R. B., Hoffman, Y., & Courtois, D. 2013, AJ, 146, 69

Cybulski, R., Yun, M. S., Fazio, G. G., & Gutermuth, R. A. 2014, MNRAS, 439, 3564

Dálya, G., Galgóczi, G., Dobos, L., et al. 2018, MNRAS, 479, 2374

de Vaucouleurs, G. 1953, AJ, 58, 30

de Vaucouleurs, G. 1956, Vistas in Astronomy, 2, 1584

de Vaucouleurs, G. 1958, Nature, 182, 1478

de Vaucouleurs, G. 1975, in Galaxies and the Universe, ed. A. Sandage, M. Sandage, & J. Kristian (Chicago Press), 557

DESI Collaboration, Adame, A. G., Aguilar, J., et al. 2023, arXiv e-prints, arXiv:2306.06308

Dressler, A. 1980, ApJ, 236, 351

Drinkwater, M. J., Phillipps, S., Jones, J. B., et al. 2000, A&A, 355, 900

Ducoin, J. G., Corre, D., Leroy, N., & Le Floch, E. 2020, MNRAS, 492, 4768

Einasto, J., Corwin, H. G., J., Huchra, J., Miller, R. H., & Tarenghi, M. 1983, Highlights of Astronomy, 6, 757

Einasto, J., Hütsi, G., Einasto, M., et al. 2003, A&A, 405, 425

Einasto, J., Joeveer, M., & Saar, E. 1980, MNRAS, 193, 353

Einasto, M. 1992, MNRAS, 258, 571

Einasto, M. & Einasto, J. 1987, MNRAS, 226, 543

Einasto, M., Einasto, J., Tenjes, P., et al. 2024, A&A, 681, A91

Einasto, M., Gramann, M., Park, C., et al. 2018, A&A, 620, A149

Einasto, M., Kipper, R., Tenjes, P., et al. 2021, A&A, 649, A51

Einasto, M., Lietzen, H., Gramann, M., et al. 2017, A&A, 603, A5

Einasto, M., Lietzen, H., Gramann, M., et al. 2016, A&A, 595, A70

Einasto, M., Liivamägi, L. J., Tago, E., et al. 2011a, A&A, 532, A5

Einasto, M., Liivamägi, L. J., Tempel, E., et al. 2011b, ApJ, 736, 51

Einasto, M., Tago, E., Jaaniste, J., Einasto, J., & Andernach, H. 1997, A&AS, 123, 119

Einasto, M., Tago, E., Saar, E., et al. 2010, A&A, 522, A92

Einasto, M., Tenjes, P., Gramann, M., et al. 2022, A&A, 666, A52

Euclid Collaboration, Scaramella, R., Amiaux, J., et al. 2022, A&A, 662, A112

Fairall, A. P., Paverd, W. R., & Ashley, R. P. 1994, in Astronomical Society of the Pacific Conference Series, Vol. 67, Unveiling Large-Scale Structures Behind the Milky Way, ed. C. Balkowski & R. C. Kraan-Korteweg, 21

For, B. Q., Spekkens, K., Staveley-Smith, L., et al. 2023, MNRAS, 526, 3130

Fujita, Y. 2004, PASJ, 56, 29

Galárraga-Espinosa, D., Garaldi, E., & Kauffmann, G. 2023, A&A, 671, A160
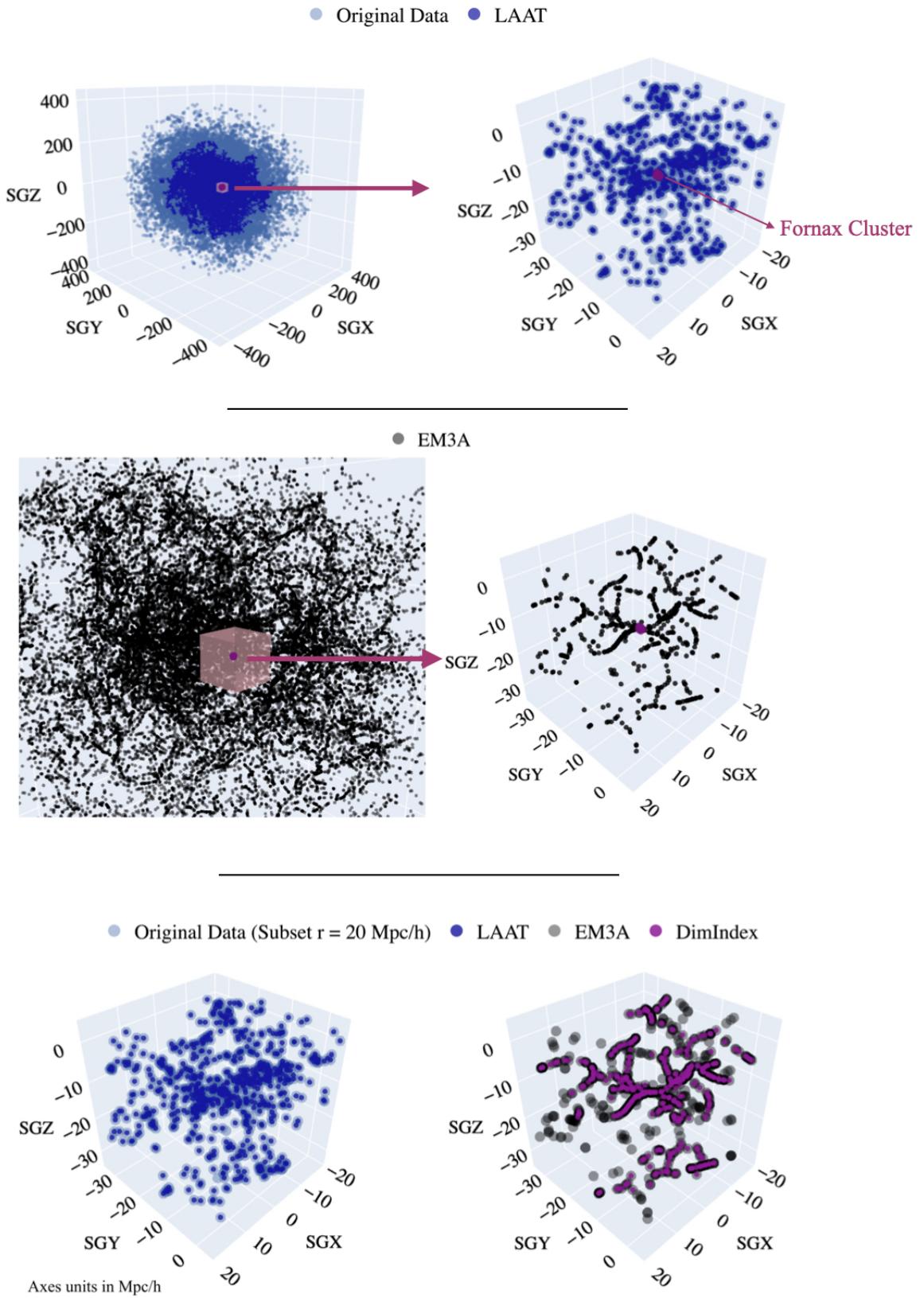
Geller, M. J. & Huchra, J. P. 1989, Science, 246, 897

Gott, J. Richard, I., Jurić, M., Schlegel, D., et al. 2005, ApJ, 624, 463
Gunn, J. E. & Gott, J. Richard, I. 1972, ApJ, 176, 1
Haines, C. P., Busarello, G., Merluzzi, P., et al. 2018, MNRAS, 481, 1055
Haines, C. P., Merluzzi, P., Mercurio, A., et al. 2006, MNRAS, 371, 55
Hatamkhani, N., Kraan-Korteweg, R. C., Blyth, S. L., Said, K., & Elagali, A. 2023, MNRAS, 522, 2223
Heß, S., Kitaura, F.-S., & Gottlöber, S. 2013, MNRAS, 435, 2065
Hoosain, M., Blyth, S.-L., Skelton, R. E., et al. 2024, MNRAS, 528, 4139
Huchra, J. P. & Geller, M. J. 1982, ApJ, 257, 423
Huchra, J. P., Macri, L. M., Masters, K. L., et al. 2012, ApJS, 199, 26
Hunter, J. D. 2007, Computing in Science & Engineering, 9, 90
Icke, V. 1973, A&A, 27, 1
Inc., P. T. 2015, Collaborative data science
Jõeveer, M., Einasto, J., & Tago, E. 1978, MNRAS, 185, 357
Jones, D. H., Read, M. A., Saunders, W., et al. 2009, MNRAS, 399, 683
Jones, J. E. & Jones, B. J. T. 1980, MNRAS, 191, 685
Kauffmann, G., White, S. D. M., Heckman, T. M., et al. 2004, MNRAS, 353, 713
Kitaura, F. S. 2013, MNRAS, 429, L84
Kitaura, F. S., Sinigaglia, F., Balaguera-Antolínez, A., & Favole, G. 2024, A&A, 683, A215
Kleiner, D., Serra, P., Maccagni, F. M., et al. 2021, A&A, 648, A32
Kourkchi, E. & Tully, R. B. 2017, ApJ, 843, 16
Kraan-Korteweg, R. C., Cluver, M. E., Bilicki, M., et al. 2017, MNRAS, 466, L29
Kraljic, K., Arnouts, S., Pichon, C., et al. 2018, MNRAS, 474, 547
Kuchner, U., Haggar, R., Aragón-Salamanca, A., et al. 2022, MNRAS, 510, 581
Kuutma, T., Tamm, A., & Tempel, E. 2017, A&A, 600, L6
Lavaux, G. & Hudson, M. J. 2011, MNRAS, 416, 2840
Libeskind, N. I., Hoffman, Y., & Gottlöber, S. 2014, MNRAS, 441, 1974
Libeskind, N. I., van de Weygaert, R., Cautun, M., et al. 2018, MNRAS, 473, 1195
Lietzen, H., Tempel, E., Liivamägi, L. J., et al. 2016, A&A, 588, L4
Liivamägi, L. J., Tempel, E., & Saar, E. 2012, A&A, 539, A80
Lopes, P. A. A., Ribeiro, A. L. B., & Brambila, D. 2024, MNRAS, 527, L19
Makarov, D. & Karachentsev, I. 2011, MNRAS, 412, 2498
Malavasi, N., Sorce, J. G., Dolag, K., & Aghanim, N. 2023, A&A, 675, A76
Marasco, A., Poggianti, B. M., Fritz, J., et al. 2023, MNRAS, 525, 5359
Mei, S., Hatch, N. A., Amodeo, S., et al. 2023, A&A, 670, A58
Mohammadi, M. & Bunte, K. 2020, in Intelligent Data Engineering and Automated Learning – IDEAL 2020, ed. C. Analide, P. Novais, D. Camacho, & H. Yin (Cham: Springer International Publishing), 12–24
Nasonova, O. G., de Freitas Pacheco, J. A., & Karachentsev, I. D. 2011, A&A, 532, A104
Peebles, P. J. E. 2023, MNRAS, 526, 4490
Pfeifer, S., Libeskind, N. I., Hoffman, Y., et al. 2022, MNRAS, 514, 470
Phillipps, S. & Davies, J. 1992, in Astrophysics and Space Science Library, Vol. 174, Digitised Optical Sky Surveys, ed. H. T. MacGillivray & E. B. Thomson, 295
Ramsøy, M., Slyz, A., Devriendt, J., Laigle, C., & Dubois, Y. 2021, MNRAS, 502, 351
Román, J. & Trujillo, I. 2017, MNRAS, 468, 703
Santiago-Bautista, I., Caretta, C. A., Bravo-Alfaro, H., Pointecouteau, E., & Andernach, H. 2020, A&A, 637, A31
Sarron, F., Adami, C., Durret, F., & Laigle, C. 2019, A&A, 632, A49
Schaye, J., Crain, R. A., Bower, R. G., et al. 2015, MNRAS, 446, 521
Shapley, H. 1930, Harvard College Observatory Bulletin, 874, 9
Skrutskie, M. F., Cutri, R. M., Stiening, R., et al. 2006, AJ, 131, 1163
Sorce, J. G., Gottlöber, S., Yepes, G., et al. 2016, MNRAS, 455, 2078
Sousbie, T. 2011, MNRAS, 414, 350
Springel, V. 2005, MNRAS, 364, 1105
Taghribi, A., Bunte, K., Smith, R., et al. 2023, IEEE Transactions on Knowledge and Data Engineering, 35, 6014
Tegmark, M., Blanton, M. R., Strauss, M. A., et al. 2004, ApJ, 606, 702
Tempel, E., Kipper, R., Tamm, A., et al. 2016, A&A, 588, A14
Tempel, E., Stoica, R. S., Martínez, V. J., et al. 2014, MNRAS, 438, 3465
Tully, R. B. 1987, ApJ, 321, 280
Tully, R. B., Courtois, H., Hoffman, Y., & Pomarède, D. 2014, Nature, 513, 71
Tully, R. B., Courtois, H. M., Dolphin, A. E., et al. 2013, AJ, 146, 86
Tully, R. B. & Fisher, J. R. 1987, Atlas of Nearby Galaxies (Cambridge University Press)
Tully, R. B., Rizzi, L., Shaya, E. J., et al. 2009, AJ, 138, 323
van de Weygaert, R. & Bond, J. R. 2008, in A Pan-Chromatic View of Clusters of Galaxies and the Large-Scale Structure, ed. M. Plionis, O. López-Cruz, & D. Hughes, Vol. 740 (Springer), 335
van de Weygaert, R. & Schaap, W. 2009, in Data Analysis in Cosmology, ed. V. J. Martínez, E. Saar, E. Martínez-González, & M. J. Pons-Bordería, Vol. 665 (Springer), 291–413
Venturi, T., Giacintucci, S., Merluzzi, P., et al. 2022, A&A, 660, A81
Vogelsberger, M., Genel, S., Springel, V., et al. 2014, MNRAS, 444, 1518
Vulcani, B., Poggianti, B. M., Fritz, J., et al. 2015, ApJ, 798, 52
White, S. D. M. & Rees, M. J. 1978, MNRAS, 183, 341
White, S. D. M. & Silk, J. 1979, ApJ, 231, 1
Winkel, N., Pasquali, A., Kraljic, K., et al. 2021, MNRAS, 505, 4920
Zabludoff, A. I. & Mulchaey, J. S. 1998, ApJ, 496, 39
Zeldovich, I. B., Einasto, J., & Shandarin, S. F. 1982, Nature, 300, 407
Zel'dovich, Y. B. 1970, A&A, 5, 84
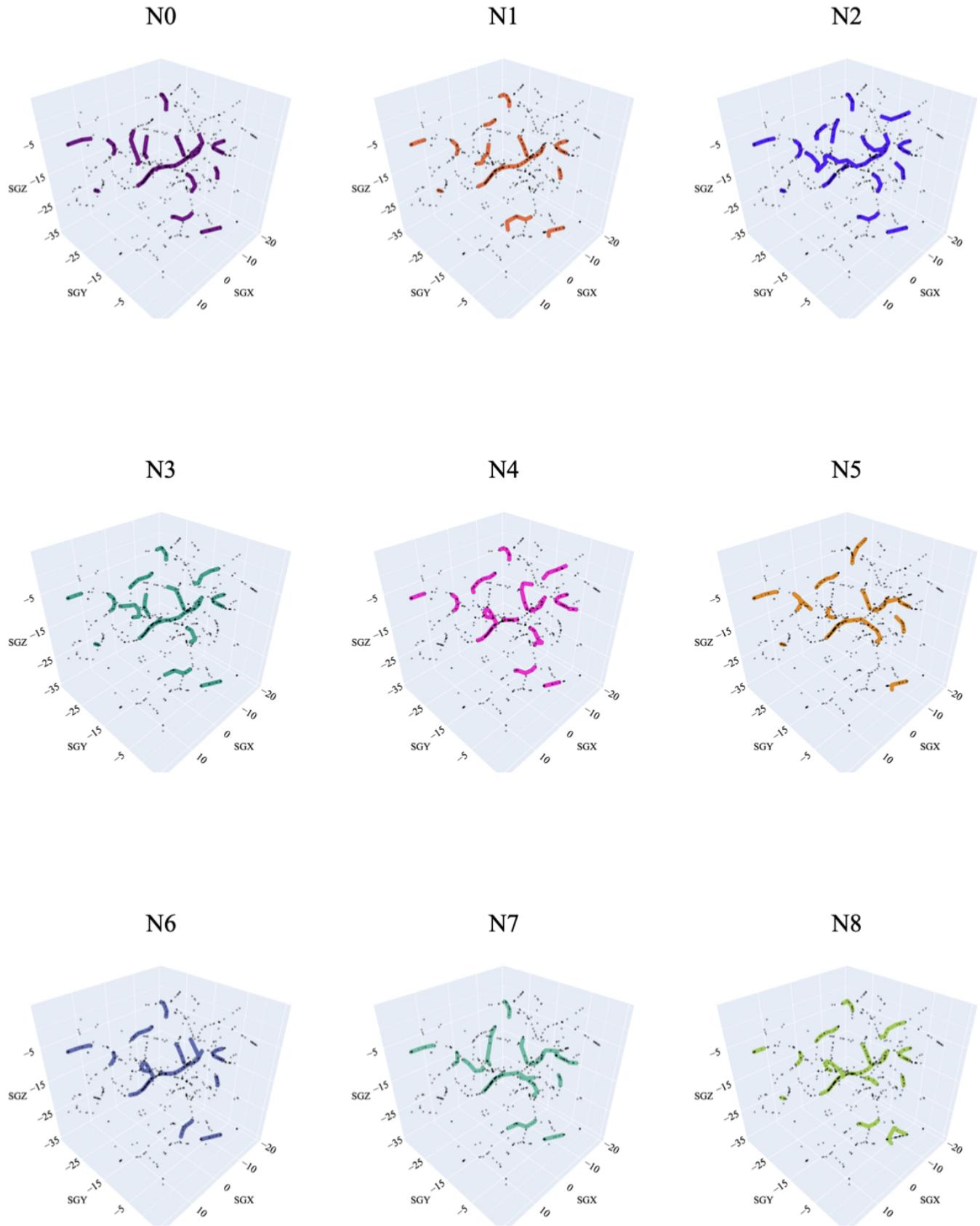
Table A.1. Input parameters for algorithms in 1-DREAM.

Algorithm.	Parameter	Value	Description
LAAT	$r \in \mathbb{R}$	3	Neighbourhood radius
	$\zeta \in \mathbb{R}$	0.05	Evaporation rate
	$\kappa \in \mathbb{R}$	0.8	Shape v. Pheromone
	$\omega \in \mathbb{R}$	10	Inverse temperature
	$\gamma \in \mathbb{R}$	0.05	Deposited pheromone
	$F \in \mathbb{R}$	10	Pheromone threshold
	$N_{epoch} \in \mathbb{N}$	100	Number of Epochs
	$N_{steps} \in \mathbb{N}$	1200	Steps per epoch
	$N_{ants} \in \mathbb{N}$	5	Number of Agents
EM3A+	$r \in \mathbb{R}$	3	Neighbourhood radius
	$\eta \in \mathbb{R}$	0.1	Learning rate
	$N_s \in \mathbb{N}$	100	Number of steps
	$N_g \in \mathbb{N}$	10	Number of generations
DimIndex	$r \in \mathbb{R}$	3	Neighbourhood radius
	$\tau \in \mathbb{N}$	5	Filtering threshold
MMCrawling	$r \in \mathbb{R}$	3	Neighbourhood radius
	$\beta \in \mathbb{R}$	0.5	Jumping tolerance

Appendix A:

In this section, we present a 3D visualisation of the results from 1-DREAM and tabulate the adopted input parameters in Table A.1. Fig. A.1 depicts the results from LAAT, EM3A, and DimIndex, followed by the results from MMCrawling in Fig. A.2. Table A.2 is a tabular presentation for Fig. 8.

Fig. A.1. Results of LAAT, EM3A, and DimIndex on our data. *Top panel*: 3D representation of the original dataset by T16a (*left*) and the extracted subset (*right*) are denoted in light blue. Results from LAAT are depicted in dark blue; *Middle panel*: 3D representation of the results from EM3A on a zoomed-in perspective of the original dataset (*left*) and its extracted subset (*right*); *Lower panel*: description is the same as that of the top panels, but now includes results from DimIndex, which is indicated in magenta.

Axes units in Mpc/h

Fig. A.2. 3D representation of the results from nine iterations of MMCrawling, continued from Fig. 3.

Table A.2. Galaxy population in filaments around the Fornax-Eridanus Complex

Distance Mpc/h	N_{gal} (ETGs)			N_{gal} (LTGs)		
	Total	Groups	Pristine	Total	Groups	Pristine
(1)		(2)			(3)	
0.5	56	50	6	40	31	9
1.0	39	34	5	94	64	30
1.5	34	27	7	71	51	20
2.0	17	9	8	62	34	28
2.5	9	5	4	29	17	12
3.0	7	5	2	21	7	14

Notes. Column 1 – Histogram bin; Column 2 – Total number of ETGs in filaments, of which belong to groups/clusters, and pristine environments of filaments ; Column 3 – Total number of LTGs in filaments, of which belong to groups/clusters, and pristine environments of filaments.